(e, 2e) spectroscopy

M. A. Coplan

Institute for Physical Science and Technology, University of Maryland, College Park, Maryland 20742

J. H. Moore

Department of Chemistry and Biochemistry, University of Maryland, College Park, Maryland 20742

J. P. Doering

Department of Chemistry, Johns Hopkins University, Baltimore, Maryland 21218

Most of our knowledge of the electronic structure of atoms and molecules is derived from excitation energies and transition probabilities. These observable quantities are related to the electronic wave functions by integrals over unmeasured variables. Another observable more directly related to the wave function than energy or transition probability is the single-electron momentum density, the probability that an electron in a well-defined orbital has a given value of momentum. Over the last twenty years a technique has been developed for measuring momentum densities in atoms and molecules. The technique, $(e,2e)$ spectroscopy, is based on electron-impact ionization with complete determination of the momentum of both incoming and outgoing electrons. The conditions necessary to extract momentum-density information from the ionization experiments are examined and related to general theories of electron scattering. Different experimental arrangements are reviewed and momentum-density results from selected examples are discussed.

CONTENTS

I. INTRODUCTION

A. General comments on (e, 2e) processes

$(e,2e)$ spectroscopy refers specifically to electron-impact ionization experiments in which a fast projectile electron is used to eject a bound electron from an atomic or molecular target with the simultaneous detection of the two out-going electrons. The experimental parameters are adjusted to provide a reasonably straightforward relation between the measured differential ionization cross section and the momentum-density function of the target electron. The momentum-density function $\rho(\mathbf{q})$ is the square modulus of the momentum-space wave function, which itself is the momentum-space transform of the more familiar position-space wave function. By analogy with the charge density, the momentum density is the probability that an electron has a particular momentum per unit volume of momentum space. The integral of this quantity when integrated over all momentum space is unity.

The $(e,2e)$ reaction can be illustrated by a classical model. Consider first a single electron, fixed in space, that is struck by a second, projectile electron with kinetic energy E_0 and momentum $\mathbf{p}_0$. Energy and momentum are conserved in the collision so that if the energy (E_a) and momentum ($\mathbf{p}_a$) of the scattered projectile are measured, the energy (E_b) and momentum ($\mathbf{p}_b$) of the ejected electron are determined. The momentum transferred to the target electron, $\mathbf{p}_0-\mathbf{p}_a$, is equal to $\mathbf{p}_b$. Now consider the target electron to be one of a number of electrons in a molecule, with binding energy IP, and suppose that at the instant of collision it is moving in some arbitrary direction with momentum $\mathbf{q}$. Under these circumstances,

 0034-6861/94/66(3)/985(30)/$08.00

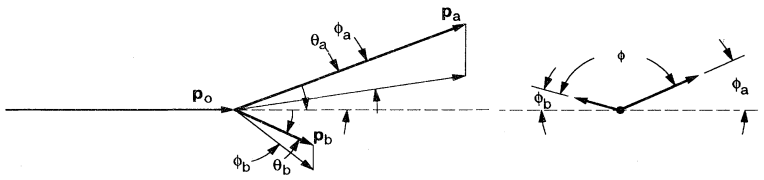

FIG. 1. Two views of the kinematics of an $(e,2e)$ reaction. The incident electron has momentum $\mathbf{p}_0$. The scattered electron has momentum $\mathbf{p}_a$, and its direction with respect to the incident electron is defined by the polar angle θ_a and out-of-plane angle ϕ_a. The ejected electron has momentum $\mathbf{p}_b$, and its direction with respect to the incident electron is defined by the polar angle θ_a and out-of-plane angle ϕ_b. The angle ϕ is defined as $\pi-(\phi_a+\phi_b)$.

the momentum of the target electron after the collision is the vector sum of the momentum transferred to it by the projectile and the momentum it had at the instant of the collision. In order that momentum be conserved, the residual ion must recoil from the collision with momentum equal and opposite to $\mathbf{q}$. The geometry of this case is shown in Fig. 1. Furthermore, the sum of the kinetic energies of the projectile and target electrons after the collision is less than the kinetic energy of the incident electron by precisely the value of the binding energy of the target electron. The implications of these facts are profound. If one can establish the momentum of the incident electron before and after the collision, along with the momentum of the target electron after its ejection, it is possible to calculate the momentum of the target electron at the instant of collision. Additionally, the determination of the kinetic energies of the electrons after the collision is sufficient to establish the origin of the target electron. By its very nature, the experiment is a coincidence experiment because it is necessary that the scattered and ejected electrons originate from the same collision event. By performing the experiment over and over with a collection of identical atoms or molecules, and accepting for analysis those coincident electrons with a single ionization potential, one can obtain a momentum-density function. This function is the square of the momentum-space wave function for the system, and in principle can be calculated by solving the Schrödinger equation in momentum space or by taking the Fourier transform of the position-space function. The momentum-space wave function, and by extension, the momentum density, retain the full symmetry properties of the position-space wave function. The ability to measure momentum densities unambiguously, combined with binding energy selectivity, is, from our perspective, one of the most important and useful features of the $(e,2e)$ experiment.

When attempting to understand the properties of atoms and molecules one can choose between two extreme points of view. On the one hand, there are simple models that explain the properties of molecules in terms of the arrangement of a small number of valence electrons. These originated with the theories of Higgins (1789) and Dalton (1808), who postulated the aggregation of small numbers of atoms into molecular units, and culminated in the electron-pair bond theory put forward by Lewis (1916). These essentially static pictures have been very effective in organizing the large body of physical and chemical experimental data on atoms and molecules and, perhaps more importantly, have proved useful for predicting the properties of new molecules. By contrast, there is the quantum-mechanical description that takes into account the full complexity of many-electron atoms and molecules, and allows for the calculation of certain global properties, such as total energy, dipole moment, and polarizability, but mostly fails to provide the simple explanations of chemical and physical properties of atoms and molecules necessary for predicting even such fundamental properties as acidity, basicity, or reactivity. Experimental momentum densities can provide the bridge between the simple static view of electronic structure and the description provided by quantum mechanics. Momentum densities contain a degree of detail beyond the quantities that are routinely calculated with quantum mechanics, and incorporate a measure of the complexity inherent in the dynamics of electron motion. The densities can also be interpreted in a way that is fully compatible with well established qualitative models of how electrons are arranged in atoms and molecules.[1]

With respect to the chemical and physical properties of atoms and molecules, very small differences in the electronic structure of the outer valence electrons are responsible for profound differences in properties. This is the difficulty that quantum theorists face in calculating properties that can be measured experimentally. A wave function that gives the total electronic energy of a molecule to an accuracy of a small fraction of a percent can give completely erroneous results when used to predict bond strengths, dipole moments, or polarizabilities. Experiments are equally challenging. Attempts to measure the changes in electron density associated with the formation of a bond between atoms have generally shown the differences to be of the order of the uncertainties in

[1]For a further discussion of this see Julg, A., 1980, *La Liason Chimique,* Collection Encyclopédique, Que Sais-Je? (Universitaires de France, Paris, France).

the density measurements themselves. The $(e,2e)$ experiment was initially seen as a way of measuring, with high precision, orbital-specific momentum densities that could be directly related to quantum-mechanical calculations. From these momentum densities a clearer picture of electronic structure was to emerge. To appreciate the experimental and theoretical demands of this proposition, it is worthwhile to estimate the precision and accuracy necessary to recover the details of electron momentum densities from an $(e,2e)$ experiment. Consider a comparison of the hydrogen atom and the hydrogen molecule. Calculated momentum densities for the $1s$ orbital of H and the $1s\sigma_g$ state of H_2 are shown in Fig. 2, both spherically averaged and scaled to 1 at the origin. For atomic hydrogen, the calculation is exact, while for H_2 the calculation uses a wave function that gives a total electronic energy within a few percent of the experimental energy. As can be seen from the figure, the differences in the densities are of the order of ten percent even though in one case we are considering an atom and in the other a two-electron diatomic molecule. The general conclusion from this simple example is that momentum-density measurements require a combined precision and accuracy of a few percent to distinguish between isolated atoms and atoms bound to each other in a molecule. To further elaborate on this point, it is essential to recognize that the precision of a momentum-density measurement depends on the relative precision of $(e,2e)$ cross-section measurements. Because $(e,2e)$ cross sections are small, high precision implies long counting times and frequent calibratons of the detectors and scattering geometry. On the other hand, the accuracy of a momentum-density measurement depends on the very nature of electron-impact ionization and the ability to experimentally isolate from all the many kinds of electron collisions those that result in the ejection of an electron from the target without interfering interactions. In this regard we are fortunate in being able to draw on the large body of experimental and theoretical results on electron-impact ionization that have identified many of the interactions that exist. From an understanding of the interactions, it has been possible to choose experimental conditions that give cross-section data from which momentum densities can be derived with the requisite accuracy of a few percent.

If only symmetry information is sought from the momentum densities, the requirements on precision and accuracy are considerably reduced. Because symmetries can be obtained from a knowledge of the positions of the momentum-density nodes, precision and accuracy from several percent to as much as twenty percent is often sufficient.

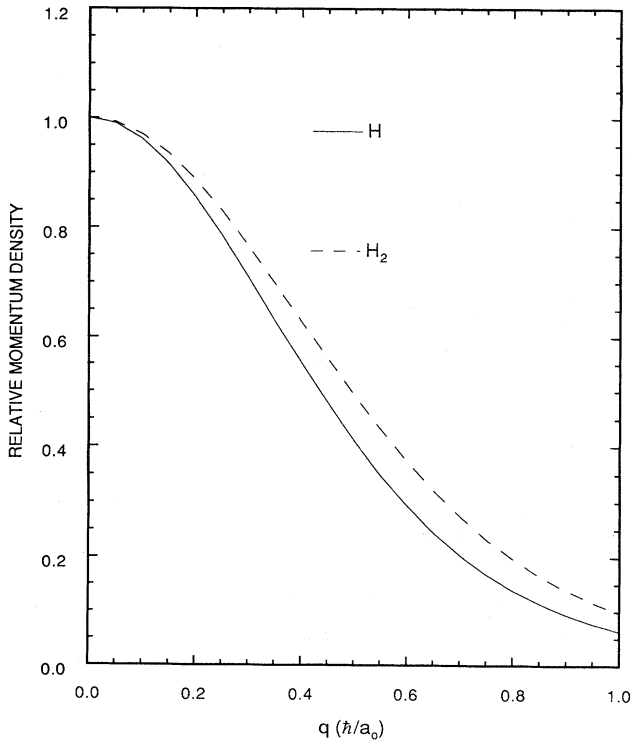

FIG. 2. Calculated momentum densities for the $1s$ state of the hydrogen atom and the $1s\sigma_g$ state of the hydrogen molecule. The two densities have been made equal at $q=0$.

B. The development of (e,2e) spectroscopy

Ernest Rutherford's discovery of the atomic nucleus using alpha particles marks the beginning of modern scattering experiments. Rutherford (1911) realized that a measurement of the angular distribution of scattered particles would give information about the internal structure of the scatterer. Since 1911, many experimental variations on Rutherford's basis idea have been used for the study of nuclei, atoms, molecules, and solids. $(e,2e)$ spectroscopy, at 20 years of age, is one of the younger scattering techniques in atomic physics.

The idea for an atomic $(e,2e)$ spectroscopic experiment can be traced directly to the $(p,2p)$ experiment of Chamberlain and Segré (1952) in which bombardment of lithium by 340 MeV protons was observed to produce pairs of protons emitted approximately 90° to each other in the laboratory frame. These proton pairs were identified to be the result of binary collisions between the incident proton and a proton within the nucleus. If the target proton were initially at rest with zero binding energy, the pair would be emitted at exactly 90°. However, the inelasticity introduced by the finite binding energy causes the mean included angle to be slightly less than 90°. The initial momentum density of the target proton is reflected in a distribution of angles about the mean. $(p,2p)$ experiments were subsequently developed into a tool for the investigation of nuclear structure (Riou, 1965).

In a discussion of the $(p,2p)$ reaction, McCarthy (1965) showed that in the Born approximation, the $(p,2p)$ reaction matrix elements are separable into two factors: the Fourier transform of the interaction potential and the Fourier transform of the initial bound-state wave func-

tion of the knocked-out proton, both with respect to the momentum transferred from the projectile. Thus, in principle, information about the initial wave function of the proton within the nucleus could be obtained from experiment.

Smirnov and Neudachin (1966) first suggested that an equivalent experiment should be possible for atomic- and molecular-orbital electrons. They pointed out that the cross section for such an event should be proportional to the square of the Fourier transform of the bound-state wave function of the ejected electron. The first analysis of such a hypothetical experiment was given by Glassgold and Ialongo (1968) who showed that, by analogy with the nuclear $(p,2p)$ reaction, single ionization of atoms by high-energy incident electrons should produce an observable number of binary collisions between the incident electron and one of the atomic electrons. If the energies and momenta of these emitted electrons could be measured in a coincidence experiment, it would be possible to determine experimentally the momentum density of electrons from a single, known atomic orbital by determining the variation of cross section with angle.

The experimental feasibility of binary $(e,2e)$ experiments was first demonstrated by Amaldi *et al.* (1969) on carbon-film targets. Camilloni *et al.* (1972) performed the first $(e,2e)$ momentum-density experiment on electrons ejected from the K and L shells of carbon using a carbon-foil target. The first $(e,2e)$ measurements on a gas-phase target used argon (Weigold *et al.*, 1973). These developments led to a great deal of theoretical and experimental work. Initially, the most important problem was to determine the range of validity of the theoretical approximations necessary for the interpretation of the experimental data. Once satisfactory agreement of theory and experiment was obtained for simple atomic systems, the $(e,2e)$ experiment was applied to a wide variety of more complicated atoms and molecules.

In the past 20 years $(e,2e)$ spectroscopy has evolved from a way of confirming the results of routine momentum-density calculations to a means for investigating the details of electronic structure with a degree of detail accessible only to the most advanced calculations. The present review is organized to give a primarily experimental view of $(e,2e)$ spectroscopy. We first discuss ionization cross sections and kinematic regimes to locate those conditions suitable for $(e,2e)$ spectroscopy among the wide variety of electron-impact ionization processes. Second, we discuss the theoretical basis of $(e,2e)$ measurements. Third, we discuss experimental techniques. Finally, we discuss the interpretation of the data and review a selection of experimental results. As most work to the present time has been carried out on gas-phase targets, we shall concentrate on gas-phase experiments. Our presentation draws heavily on the many previous excellent reviews of various aspects of $(e,2e)$ experiments, including those of Weigold (1984), Ehrhardt *et al.* (1986), Byron and Joachain (1989), McCarthy and Weigold (1989), Lahmam-Bennani (1991), and Leung (1991).

II. IONIZATION CROSS SECTIONS AND KINEMATIC REGIMES

A. Kinematics

Electron-impact ionization of a target atom or molecule M, assumed to be initially in its ground state, can be described completely by the reaction

$$e_0(E_0,\mathbf{p}_0)+M\rightarrow M^+(s_{i\alpha},\mathbf{p})+e_a(E_a,\mathbf{p}_a)+e_b(E_b,\mathbf{p}_b)\ ,$$

where the E_j are the electron kinetic energies $(j=0,a,b)$ with E_0 the energy of the incident electron. Similarly, the $\mathbf{p}$'s are the momenta of the products, and $s_{i\alpha}$ specifies the final state of the ionized target. The subscript $i\alpha$ specifies the ionized electron i and the final state α of the ion. If the outgoing electrons have very different energies, it is common to assign the indices a to the "fast," "scattered," or "scattered primary" electron and b to the "slow" or "ejected" electron even though the electrons are indistinguishable. Conservation of energy requires

$$E_0=E_a+E_b+IP_{i\alpha}\ ,$$

where $IP_{i\alpha}$ is the target ionization potential for final state $s_{i\alpha}$. The kinetic energy available is $E_0-IP_{i\alpha}$, and it can be shared between the two outgoing electrons in any proportion. When $E_a=E_b$ the energy sharing is *symmetric*. For *asymmetric* events $E_a\neq E_b$.

If the target atom or molecule is at rest, it has no net momentum. After subtraction of the momentum transferred to the ejected electron by the incident electron, the momenta of the residual ion and ejected electron must also sum to zero, so that the momentum of the residual ion $\mathbf{p}$, the recoil momentum, is equal and opposite to $\mathbf{q}$, the momentum of the ejected electron at the instant of ionization. The recoil energy of the residual ion, $p^2/2m_{ion}$, is small compared to that of the ejected electron and is neglected in the energy conservation equation. The conservation of momentum relation is

$$\mathbf{p}_0=\mathbf{p}_a+\mathbf{p}_b-\mathbf{q}\ .$$

Additionally, the momentum vectors of the outgoing electrons are not necessarily coplanar with that of the incident electron because q can have many different directions.

For the experimental determination of electron momentum, it is necessary to know the velocities of the electrons and their directions of motion. The velocities are established from the kinetic energies and the directions of motion, generally specified by polar angles, θ_a and θ_b, and azimuthal angles ϕ_a and ϕ_b, with respect to the direction of the incident electron (Fig. 1). In addition to the relation between E_a and E_b, collisions can also be *coplanar* or *noncoplar* depending on the azimuthal angles. Successful $(e,2e)$ experiments have been carried out in all geometries, with the symmetric noncoplanar the one

most frequently used in momentum-density measurements.

Next we consider the ranges of the energies and angles that are typical of electron-impact ionization experiments. It is convenient to divide the incident-electron velocity into slow, intermediate, and fast regions with respect to the orbital velocity of the target electron in the atom or molecule. Likewise, the velocities of the ejected electron can be divided into the same three regions.

Three of the kinematic combinations are sufficiently common to be given specific designations. The *threshold* regime corresponds to incident-electron velocities just sufficient to yield scattered and ejected electrons with near-zero velocity. The *dipole* regime derives its name from the close connection between photoabsorption and small-angle electron scattering (Inokuti, 1971; Brion, 1975; Hamnett *et al.*, 1976). The *binary* regime corresponds to close, billiard-ball-like collisions between the incident and target electrons with a large amount of momentum transferred from the incident electron to the ejected electron.

B. Energy sharing

Ionizing collisions can also be classified according to the relative magnitude of the momentum transferred to the target. If $\hbar\mathbf{k}_0$ is the momentum of the incident electron before the collision and $\hbar\mathbf{k}_a$ its momentum after the collision, the momentum transfer $\hbar\mathbf{K}$ is defined as $(\hbar\mathbf{k}_0-\hbar\mathbf{k}_a)$. Momentum transfer and scattering angle θ_a are related by

$$K^2=k_0^2-2k_0k_a\cos\theta_a+k_a^2 ,$$

where $\hbar$ has been suppressed to simplify the notation. Small momentum transfer collisions correspond to small angles of scatter. Ionizing collisions with momentum transfers of the order of $\hbar/a_0$ (one unit of momentum in atomic units) are more probable. For these collisions the momentum transferred to the target is just sufficient to knock out a valence electron. They have been investigated in great detail with atomic targets at both intermediate and fast incident-electron velocities (Ehrhardt *et al.*, 1986).

High-velocity ionizing collisions in which the scattered electron is deviated through a large angle correspond to large values of momentum transfer. It is these collisions that are the most useful for momentum-density measurements by (e,2e) spectroscopy. Unfortunately, they are also the least probable of all ionizing collisions.

The Bethe surface is a particularly useful representation of the range of kinematics that apply to electron collisions (Inokuti, 1971). The surface is derived from the expression for the double-differential, electron-scattering cross section using the Born approximation for the incident- and scattered-electron wave function. The cross section calculated in this way is a product of two factors, a kinematic term that is a function of the momentum transferred from the incident electron to the target and a structure term, the generalized oscillator strength (GOS). The GOS is analogous to the optical dipole oscillator strength, and is a function of the initial and final states of the target.

$$\mathrm{GOS}=(E_n/Q)|\varepsilon_n(K)|^2 ,$$

where E_n is the excitation energy of the target, Q is the energy transfer from the incident electron, and K is the magnitude of the momentum-transfer wave vector. $\varepsilon_n(K)$ is defined by

$$\varepsilon_n(\mathbf{K})=\left\langle \Psi_n \left| \sum_{i=1}^{N} \exp(i\mathbf{K}\cdot\mathbf{r}_i) \right| \Psi_0 \right\rangle ,$$

where Ψ_n is the wave function for the final state of the target, Ψ_0 is the initial-state target wave function, and the sum is over all of the N electrons of the target.

The general form of the surface adapted from Inokuti (1971) is shown in Fig. 3, where the derivative of the generalized oscillator function with respect to E_n is plotted as a function of excitation energy, (ΔE), and natural logarithm of the momentum transfer. At small momentum transfer we have the dipole regime in which excitation of the target atom or molecule is very similar to photoabsorption. As the momentum transfer increases, the generalized oscillator strength decreases with appreciable values for excitation corresponding to ejection of an electron. This is the region of the *Bethe ridge,* the binary region where the collisions most nearly correspond to the collision of two free electrons with the residual ion acting

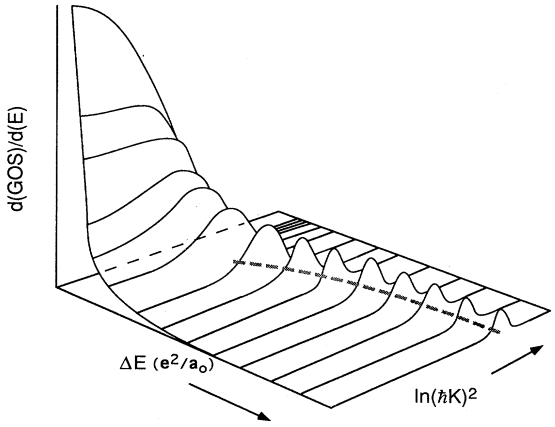

FIG. 3. Bethe surface for a model one-electron atomic target adapted from Inokuti (1971). The vertical axis is the derivative of the generalized oscillator strength (GOS) with respect to the excitation energy. Energy ΔE is in units of twice the ionization potential of hydrogen (e^2/a_0), and momentum transfer is in units of $\hbar/a_0$. For small values of momentum transfer, $\hbar K$, the form of the surface resembles that for photoabsorption. At large momentum transfer the only excitation that has appreciable probability is ionization. This region is dominated by the Bethe ridge, marked by the solid curved line on the base plane.

as a spectator.

The variation of the ionization cross section with energy, $d\sigma/dE$, can be obtained from integration over the angle of the double-differential cross section,

$$d^2\sigma/d\Omega dE$$

(Beaty, 1975; Shyn and Sharp, 1991). The typical result is a singly differential cross section that has maxima at threshold and at (E_0-IP), and a minimum near $(E_0-IP)/2$. Binary collisions with equal energies for the two outgoing electrons are therefore the least probable of all ionizing collisions. Most ionizing collisions occur with very asymmetric energy sharing. These collisions have been studied in detail by Ehrhardt and co-workers (e.g., Ehrhardt *et al.*, 1986) and others.

III. SCATTERING THEORY FOR (e,2e) SPECTROSCOPY

In this section we develop the theory of the $(e,2e)$ reaction in order to establish the relation between the actual experimental measurements of cross sections and momentum densities. Once the relation is established it will be possible to define the optimum set of experimental conditions necessary to extract momentum densities from the cross-section measurements. This is a particularly important issue given the high degree of accuracy needed to interpret the details of electronic structure in terms of momentum densities. The $(e,2e)$ experiment involves a measurement, for a given incident electron energy E_0, of the probability that the incident electron is scattered with energy E_a into the solid angle Ω_a, as specified by angles θ_a and ϕ_a, at the same time that the ejected electron, with energy E_b, is found at solid angle Ω_b, specified by angles θ_b and ϕ_b. This probability per unit solid angle and per unit energy is proportional to the target density and the path length of the incident electrons through the target gas. The constant of proportionality is the fourfold differential cross section, $d^4\sigma_{(e,2e)}/d\Omega_a d\Omega_b dE_a dE_b$. By convention, the solid angle Ω is treated as a single variable, not two independent variables θ and ϕ. In the measurement of an orbital momentum density, the cross section refers to a specific final state of the residual ion, so E_a and E_b are not independent. The reported cross section is then triply differential: $d^3\sigma_{(e,2e)}/d\Omega_a d\Omega_b dE_a$ or, alternatively, $d^3\sigma_{(e,2e)}/d\Omega_a d\Omega_b dE_b$. On the other hand, the fourfold differential cross section can be used to investigate branching ratios to excited states of the residual ion (Doering and Goembel, 1991; Goembel, 1992). The threefold-differential cross section specifies the orbital of the target atom or molecule from which the electron has been removed as well as the final state of the ion, so it is possible to identify the ejected electron uniquely from the collision kinematics. This application is particularly important in the measurement of "satellite" lines in the $(e,2e)$ spectrum, a topic that will be discussed later.

A large number of theoretical treatments of electron scattering exists. Our purpose here is not to review all of them in detail, but rather to arrange them in such a way that the underlying assumptions and the region of validity of each is clear. The final test of a theory is agreement with experiment. Many $(e,2e)$ experiments have been designed specifically to test theories. These experiments will also be reviewed.

A. Scattering in a central potential

The Schrödinger equation for the motion of an electron of mass m in a central potential $V(\mathbf{r})$ is

$$\left[-\frac{\hbar^2}{2\mu}\nabla^2+V(\mathbf{r})\right]X_a^{(-)}=EX_a^{(-)}\ . \tag{3.1}$$

In the limit of large r, far from the scattering center, the solution of the equation for $X_a^{(-)}$ has the form

$$X_a^{(-)}\underset{r\to\infty}{=}e^{i\mathbf{k}_0\cdot\mathbf{r}}+f_k^{(-)}(\Omega)\frac{e^{i\mathbf{k}\cdot\mathbf{r}}}{r}\ , \tag{3.2}$$

where $\mathbf{k}_0$ is the wave vector describing the incident-electron wave, and r is the magnitude of $\mathbf{r}$. The first term is the unscattered incident wave while the second term is the scattered spherical wave of amplitude $f_k^{(-)}(\Omega)$. The differential cross section into the solid angle Ω is the square of the absolute value of the amplitude of the scattered wave

$$d\sigma/d\Omega=|f_k^{(-)}(\Omega)|^2\ . \tag{3.3}$$

As well as being the solution of the Schrödinger equation with appropriate boundary conditions, $X_a^{(-)}$ is also the solution of an integral equation. The form of the integral equation allows one to write $X_a^{(-)}$ as a series in powers in $V(\mathbf{r})$ and evaluate corrections to various approximations. The integral equation is

$$X_a^{(-)}=e^{i\mathbf{k}_0\cdot\mathbf{r}}-\frac{m}{2\pi\hbar^2}\int\frac{e^{i\mathbf{k}\cdot|\mathbf{r}-\mathbf{r}'|}}{|\mathbf{r}-\mathbf{r}'|}V(\mathbf{r}')X_a^{(-)}(\mathbf{r}')d\mathbf{r}'\ . \tag{3.4}$$

Since $|\mathbf{r}-\mathbf{r}'|\to r[1-(\mathbf{r}\cdot\mathbf{r}')/r^2+O(r'^2/r^2)]$ for large r, the wave function has the asymptotic form

$$X_a^{(-)}(\mathbf{r})\underset{r\to\infty}{=}e^{i\mathbf{k}_0\cdot\mathbf{r}}-\frac{m}{2\pi\hbar^2}\frac{e^{i\mathbf{k}\cdot\mathbf{r}}}{r}\int X_a^{(-)}(\mathbf{r}')V(\mathbf{r}')\times e^{-i\mathbf{k}\cdot\mathbf{r}'}d\mathbf{r}'\ , \tag{3.5}$$

where $\mathbf{k}$, the scattered wave vector, equals $k\mathbf{r}/r$. For this case of elastic scattering by a central potential, the magnitude of the scattered wave vector is equal to that of the incident wave vector, only the direction is changed so that $|\mathbf{k}|=|\mathbf{k}_0|$. Solution of Eq. (3.5) by iteration constitutes the *Born series.* The *Born approximation,* the lowest-order solution, consists of taking $X_a^{(-)}(\mathbf{r}')$ to be the plane wave $e^{i\mathbf{k}_0\cdot\mathbf{r}'}$. Then $X_a^{(-)}$ is given by

$$X_a^{(-)}(\mathbf{r}')=e^{i\mathbf{k}_0\cdot\mathbf{r}}-\frac{m}{2\pi\hbar^2}\frac{e^{i\mathbf{k}\cdot\mathbf{r}}}{r}\int e^{i\mathbf{k}_0\cdot\mathbf{r}'}V(\mathbf{r}')e^{-i\mathbf{k}\cdot\mathbf{r}'}d\mathbf{r}'\ . \tag{3.6}$$

The Born approximation is a high-energy approximation most applicable when the potential $V(\mathbf{r})$ is small compared to the kinetic energies of the projectile electron both before and after scattering.

The second-order approximation consists of using the Born approximation for $X_a^{(-)}(\mathbf{r}')$. It has the form

$$X_a^{(-)}(\mathbf{r})=e^{i\mathbf{k}_0\cdot\mathbf{r}}-\frac{m}{2\pi\hbar^2}\frac{e^{ik\cdot r}}{r}\int\int e^{i\mathbf{k}_0\cdot\mathbf{r}'}V(\mathbf{r}')V(\mathbf{r}'')\times e^{-i\mathbf{k}\cdot\mathbf{r}'}e^{-i\mathbf{k}\cdot\mathbf{r}''}d\mathbf{r}'d\mathbf{r}'' , \tag{3.7}$$

where the potential appears to second order.

Returning to the integral equation (3.5) for the scattering amplitude in the potential $V(\mathbf{r})$, the cross section for the scattering of the incident electron with wave vector $\mathbf{k}_a$ into the differential solid angle $d\Omega$ can be written

$$d\sigma/d\Omega=\frac{m^2}{4\pi^2\hbar^4}|\langle e^{i\mathbf{k}\cdot\mathbf{r}'}|V|X_a^{(-)}\rangle|^2 . \tag{3.8}$$

$\langle e^{i\mathbf{k}\cdot\mathbf{r}'}|V|X_a^{(-)}\rangle$ is not a matrix of the operator V because the two functions are not basis functions in the same representation; however, it is possible to define a matrix, called the T matrix, given by

$$T(\mathbf{k},\mathbf{k}')=\langle e^{i\mathbf{k}\cdot\mathbf{r}'}|V|X_a^{(-)}\rangle=\langle e^{i\mathbf{k}\cdot\mathbf{r}'}|T|e^{i\mathbf{k}'\cdot\mathbf{r}'}\rangle . \tag{3.9}$$

In an analogous way we can define the V matrix to be

$$V(\mathbf{k},\mathbf{k}')=\langle e^{i\mathbf{k}\cdot\mathbf{r}'}|V|e^{i\mathbf{k}'\cdot\mathbf{r}'}\rangle . \tag{3.10}$$

In the Born approximation the T matrix and V matrix are identical.

B. Electron-impact ionization

The simple introduction to electron scattering can be modified for electron-impact ionization. While the theory of scattering in a central potential is a two-body theory, electron-impact ionization involves, at the very least, three bodies: the incident electron, the target or ejected electron, and the ion core to which the target electron was bound before ionization. The cross section for ionization is differential in the angles of the scattered and ejected electrons and the energy of the ejected electron. For an N-electron atomic or molecular target the Hamiltonian includes the kinetic-energy operators for the N bound electrons, as well as the free incident electron and the interaction potentials. The potential-energy operators account for electron-core interactions as well as electron-electron interactions. General solutions of the Schrödinger equation for ionization involve the coordinates of all the electrons. For an N-electron target atom or molecule, this is computationally very difficult for all but the simplest systems, and it is necessary to seek approximate solutions.

For the purposes of $(e,2e)$ spectroscopy, we seek an experimental arrangement that allows us to extract electron-momentum densities in a simple and unambiguous way from the measurements. Figure 4 is a schematic diagram of the initial and final states of an $(e,2e)$ collision. The incident electron has momentum $\mathbf{p}_0$. It interacts with the two-electron target atom represented by a nucleus and bound electrons b and c. The various interactions, v_1 through v_6, are also shown on the figure. The interactions v_1, v_2, and v_4 are the electron-electron interactions, while v_3, v_5, and v_6 are electron-core interactions. The final state consists of scattered electron a with momentum $\mathbf{p}_a$ and ejected electron b with momentum $\mathbf{p}_b$ along with the residual ion consisting of the nucleus and electron c. The lightly shaded circles represent the target atom (nucleus and orbital electrons 2 and 3) and the residual ion (nucleus and orbital electron 3).

From considerations of electron velocities and momentum transfer, we can establish in a qualitative way the nature of the approximations that can be used in the calculation of $(e,2e)$ cross sections. At threshold, where the incident electron has just sufficient energy to eject an electron from the target, there is little distinction between the incident and target electrons, and it is unrealistic to separate the motions of the incident, scattered, and ejected electrons from that of the target electrons in the initial state. Wannier (1953) derived the energy dependence of the electron-impact ionization cross section at threshold using a classical treatment. The theory did not provide a method for calculating the ionization cross section. The Wannier threshold law was subsequently confirmed by both semiclassical (Peterkop, 1971) and quantum mechanical (Rau, 1971) derivations. Selles *et al.* (1987) modified the Wannier model to include waves beyond the ^1S in a partial wave expansion of the continuum functions. The Wannier-Peterkop-Rau

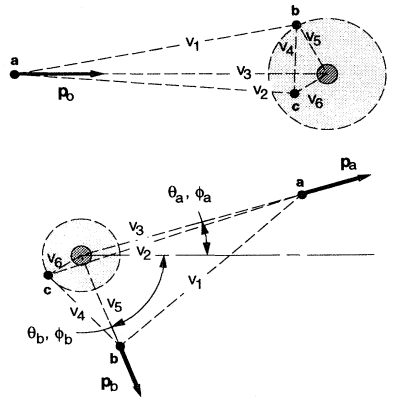

FIG. 4. Schematic diagram of the interactions between an incident electron and an atomic 2-electron target. The top drawing shows the initial state. The incident electron is labeled a and has momentum $\mathbf{p}_0$. The target electron is labeled b, and the spectator electron is c. Interactions v_1, v_2, and v_4 are electron-electron interactions, while v_3, v_5, and v_6 are electron-nucleus interactions. The final state shown in the bottom drawing shows the scattered electron with momentum $\mathbf{p}_a$ and the ejected electron with momentum $\mathbf{p}_b$. The directions of $\mathbf{p}_a$ and $\mathbf{p}_b$ are specified by θ_a, ϕ_a, θ_b, and ϕ_b.

theory was first confirmed experimentally in 1974 by Cvejanovic and Read. Experiments to test the threshold law with ever-increasing precision have continued [see, for example Hammond *et al.* (1985)]. Read (1985) has reviewed near-threshold excitation and ionization. Recently Rösel *et al.* (1992) have made absolute measurements of the triple-differential cross section for ionization of helium near threshold and have compared the results with distorted-wave-Born-approximation calculations that include a local approximation to take into account the indistinguishability of electrons (exchange). The measurements were also compared with the semiclassical calculations of Crothers (1986) and a calculation by Pan and Starace (1991) that used distorted waves for the continuum functions (see following Sec. C) and a nonlocal treatment of exchange. This latter calculation gives the best overall agreement with the experiment.

At intermediate and fast electron velocities for both low and high momentum transfer, the many-body nature of $(e,2e)$ collisions remains. Mota-Furtado and O'Mahony (1989) have performed a close-coupling calculation that treats the electron-electron interactions to all orders, but the complexity of this approach limits it to one- and two-electron atomic targets. More appropriate theories separate the motion of the incident, scattered, and ejected electrons from that of the target electrons. The initial state of the system is taken as a product of the wave function of the free-incident electron and the atomic- or molecular-target wave function, while the final state is the product of the wave functions of the scattered and ejected electrons and the residual ion. In Fig. 4, the interactions v_4, v_5, and v_6 are internal to the atom, while v_1, the interaction between the incident and target electrons, is the interaction that gives rise to ionization. Because of the disparity between the speeds of the incident, scattered, and ejected electrons and the orbital electrons of the target atom and residual ion, a common approximation is to represent the initial state as the product of the isolated target wave function and the continuum wave function of the incident electron. Correspondingly, the final state is the product of the wave function of the residual ion and the continuum wave functions of the scattered and ejected electrons. The T matrix then has the form

$$\langle X_a^{(-)}(\mathbf{k}_a,\mathbf{r}_a)X_b^{(-)}(\mathbf{k}_b,\mathbf{r}_b)\Phi_{i\alpha}|V|X_0^{(+)}(\mathbf{k}_0,\mathbf{r}_0)\Psi\rangle\ , \quad (3.11)$$

where $X_a^{(-)}$, $X_b^{(-)}$, and $X_0^{(+)}$ are the continuum wave functions for the scattered, ejected, and incident electrons, respectively. The wave function for the residual ion is $\Phi_{i\alpha}$, and the wave function for the target atom is Ψ. We assume that the target atom is in its ground state. The interaction V that couples the initial state to the final state includes the interactions between the incident electron, target electrons, and nucleus.

C. Continuum wave functions and interactions

The representation of the continuum wave functions of the incident, scattered, and ejected electrons is central to the calculation of $(e,2e)$ cross sections. In decreasing order of complexity are distorted waves, Coulomb waves, and plane waves. With three continuum electrons there is a variety of ways for them to be represented; however, consideration of particular collision geometries and kinematic regimes narrows the range of choices. The interactions that couple the initial state to the final state bear directly on the form of the continuum wave functions. Once again there are a number of choices, each appropriate for a particular kinematic regime.

1. Distorted waves

It was noted by Bethe (1940) that, for the collision of a nucleon with a nucleus, the many-body problem could be reduced to an effective two-body problem through the introduction of a complex potential of interaction that is now generally called the *optical potential.* Optical potentials have been used extensively in nuclear physics and also for electron scattering by atoms. The real part of the optical potential can be used to calculate the wave function for the incident electron. Referring to the initial state in Fig. 4, a reasonable optical potential combines the interactions v_1, v_2, and v_3 into an effective potential in which the electron moves. For the final state there are a number of choices for an effective potential depending on the relative speeds of the scattered and ejected electrons. If the ejected electron is moving slowly compared to the speed of the scattered electron, the effective potential seen by electron a is that of the neutral target (nucleus plus electrons b and c). On the other hand, if the ejected electron speed is comparable to that of the scattered electron, the effective potential is essentially that produced by the residual ion (nucleus plus electron c). If the effective potential is constructed to be spherically symmetric it becomes mathematically possible to separate the motion of the continuum electrons from the orbital electrons of the target and residual ion. A continuum-electron wave function calculated in any potential is a *distorted wave.* Complex optical potentials are used to account for inelastic processes, but the determination of an optical potential can be equivalent to the solution of the full many-body problem. There are, however, a number of approaches to the practical calculation of optical potentials. Furness and McCarthy (1973) obtained semiempirical optical potentials for electron scattering by hydrogen and argon atoms. This work was subsequently improved by McCarthy *et al.* (1977) and applied to the scattering of electrons by noble gas atoms over a wide range of incident energies. Thirumalai *et al.* (1987) have used dispersion relations to derive the generalized optical potentials for electron scattering from noble gas atoms. Though rearrangement and ionization were neglected, the approach can be generalized to in-

clude such effects.

The most complete formulation of the distorted-wave formalism used distorted waves for the incident, scattered, and ejected electrons. It has been shown by McCarthy and Weigold (1976) that the T matrix for the $(e,2e)$ process using distorted waves for all the continuum wave functions can be written as

$$\langle X_a^{(-)}(\mathbf{k}_a,\mathbf{r}_a)X_b^{(-)}(\mathbf{k}_b,\mathbf{r}_b)\Phi_{i\alpha}|V_1+V_2|X_0^{(+)}(\mathbf{k}_0,\mathbf{r}_0)\Psi\rangle \ , \tag{3.12}$$

where $X_a^{(-)}$ and $X_b^{(-)}$ are distorted waves for the scattered and ejected electrons calculated in optical potentials of the target and residual ion, and $X_0^{(+)}$ is a distorted wave for the incident electron. V_1 and V_2 incorporate the interactions of the scattered and ejected electrons with the residual ion. The neutral-target wave function is Ψ and the residual ion wave function is $\Phi_{i\alpha}$.

Zhang *et al.* (1992) have used distorted wave Born calculations to calculate $(e,2e)$ cross sections for a variety of targets and kinematic conditions. Using the notation of Eq. (3.12), $X_0^{(+)}(\mathbf{k}_0)$ was calculated in the static potential of the neutral atom, $\langle V\rangle=\langle\Psi|v_1+v_2+v_3|\Psi\rangle$. Exchange was taken into account in the calculation of $\langle V\rangle$, and $X_a^{(-)}(\mathbf{k}_a)$ and $X_b^{(-)}(\mathbf{k}_b)$ were calculated in this *static exchange potential* of the final ion state or of the neutral atom according to the scattering geometry. Elastic scattering of the incident electron by the neutral target and the two final-state electrons by the residual ion were also accounted for. The calculations neglect the polarization of the neutral atom by the incident electron and the effects of the ejected and scattered electrons on the residual ion. Polarization can, in principle, be incorporated within the distorted-wave formalism but is not considered important at the present level of calculations. Also missing from the calculations is the interaction between the ejected and scattered electrons. This *post-collision interaction* (PCI) has been considered by Popov *et al.* in a number of publications: Popov and Benayoun (1981), Popov *et al.* (1981), Popov and Erokhin (1983), and Avaldi *et al.* (1986). Within the distorted-wave formalism, post-collision interaction can be approximated by using effective charges in the calculation of the final-state distorted waves. Chant and Roos (1977) have developed a nuclear-physics computer code based on the distorted-wave impulse approximation that is appropriate for relatively large momenta where the projectile-target and projectile-residual ion interactions distort the particle waves from plane waves. The code was modified for electron-impact ionization of helium, and used to show that, at relatively large values of θ, the trajectories of the outgoing electrons are distorted to such a degree that the derived momentum densities are unreliable (Smith *et al.*, 1986). Recently this work has been extended to other energies and geometries (Dupré *et al.*, 1992; Lahmam-Bennani *et al.*, 1992).

A simplified form of the distorted-wave approximation is the *eikonal approximation.* Here, the idea is to approximate the potential felt by the incident electron by a constant potential. When this is done, the incident-electron wave function has the form of a plane wave, but with a different wavelength from the completely free electron. Experimentally, it has been found that representing the magnitude of the incident-electron wave vector by $\sqrt{2m(E_0-\mathrm{IP})}/\hbar$, in which IP is the ionization potential of the target electron, provides an improvement over simple plane waves in describing the $(e,2e)$ cross-section data in the symmetric-coplanar geometry (Camilloni *et al.*, 1978). The simple form of the eikonal continuum wave functions allows the $(e,2e)$ cross section to be separated into a part depending on the coordinates of the incident electron and a part that depends only on the coordinates of the electrons in the target, *vide infra.*

2. Coulomb waves

The next level of simplification uses Coulomb wave functions for the continuum functions in the final state. These functions are solutions of the Schrödinger equation for an electron in a potential that varies as $1/r$. The justification for this choice is that, at large distances from the residual ion, the field acting on the scattered and ejected electrons is a pure Coulomb field. When one of the final-state continuum electrons leaves the collision center with velocity much less than the other, the further simplification of using a Coulomb wave for only the slow electron is used. This assumes that the fields of the slow electron and the residual ion effectively cancel at the position of the fast electron.

A recent development of fundamental significance is the derivation by Brauner, Briggs, and Klar (1989) of the asymptotically-correct Coulomb three-body wave functions for the ejected and scattered electrons in the field of the residual ion. This is commonly referred to as the BBK theory. The importance of having the correct form of the electron wave functions at large distances from the target has been discussed by Jetzke *et al.* (1989), but at the same time the short range interactions must also be treated correctly. The synthesis of short-range and longer-range interactions to provide a complete description of scattering remains one of the principal theoretical challenges.

Another way of incorporating three-body effects into a two-body formalism is through the use of an effective charge. This approach was used by Peterkop (1963) and reviewed by Rudge (1968). The Coulomb-projected Born approximation (Geltman, 1974) is another approach to this problem.

In this discussion of Coulomb waves, it is important to note that they have not been used in any formulation of the $(e,2e)$ cross section to extract momentum densities from experimental measurements.

3. Plane waves and the impulse approximation

The simplest approximation for a continuum wave function is a plane wave; this approximation is equivalent to ignoring all forces on the incident, scattered, and ejected electrons. The interaction that couples the initial and final states of the system may incorporate all the separate interactions of the incident electron with the target electron and nucleus. If ionization can be considered to proceed by a direct collision between the incident electron and target electron with all of the momentum lost by the incident electron transferred to the ejected electron, we have the so-called *binary* regime. If, to go one step further, it can be assumed the incident electron interacts only with the ejected electron and neither affects the target nor is affected by the target, we have the *impulse* approximation. Under these circumstances the wave function for the target is the isolated-target wave function, and the final-residual-ion wave function is the isolated wave function of the ion.

Combining plane waves with the impulse approximation we have the *plane-wave impulse approximation* (PWIA) where incident, scattered, and ejected electrons are all taken to be plane waves. We expect that this approximation will be a good one when the energies of all the interactions are small compared to the kinetic energies of the incident, scattered, and ejected electrons. In practice, this means that the binding energy of the ejected electron is small compared to the kinetic energies of the incident and outgoing electrons. Because the PWIA is the approximation most often used in extracting momentum-density information from electron-impact ionization cross sections, it is useful to examine the cross section formulas in some detail.

Consider the ionization of the two electron atom of Fig. 4. The differential $(e,2e)$ cross section for this process is given by

$$d^3\sigma_{(e,2e)}/d\Omega_a d\Omega_b dE_b = \frac{m^2}{4\pi^2\hbar^4}(k_a k_b/k_0)|\langle e^{i\mathbf{k}_a\cdot\mathbf{r}} e^{i\mathbf{k}_b\cdot\mathbf{r}_b}\Phi_{i\alpha}|V(r,r_b)|\Psi e^{i\mathbf{k}_0\cdot\mathbf{r}}\rangle|^2 , \tag{3.13}$$

where $\mathbf{r}$ is the coordinate of the incident electron. Using the fact that the momentum transfer $\hbar\mathbf{K}$ is the difference between momentum of the incident electron $\hbar\mathbf{k}_0$ and the scattered electron $\hbar\mathbf{k}_a$, the cross section can be written

$$d^3\sigma_{(e,2e)}/d\Omega_a d\Omega_b = \frac{m^2}{4\pi^2\hbar^4}(k_a k_b/k_0)\left|\left\langle e^{i\mathbf{K}\cdot\mathbf{r}} e^{i\mathbf{k}_b\cdot\mathbf{r}_b}\Phi_{i\alpha}(\mathbf{r}_c)\left|-\frac{e^2}{|\mathbf{r}-\mathbf{r}_b|}\right|\Psi(\mathbf{r}_b,\mathbf{r}_b)\right\rangle\right|^2 , \tag{3.14}$$

where the Coulomb potential of interaction between the incident electron and electron b of the target is given explicitly. It is most useful to perform the integration over the variable $\mathbf{r}$ using the relation (Bethe, 1930)

$$\int|\mathbf{r}-\mathbf{r}_b|^{-1}e^{i\mathbf{K}\cdot\mathbf{r}}d\mathbf{r} = 4\pi K^{-2}e^{i\mathbf{K}\cdot\mathbf{r}_b} . \tag{3.15}$$

This leads to

$$d^3\sigma_{(e,2e)}/d\Omega_a d\Omega_b dE_b = \frac{4m^2e^4}{\hbar^4K^4}(k_a k_b/k_0)|\langle\Phi_{i\alpha}(\mathbf{r}_c)|e^{i\mathbf{q}\cdot\mathbf{r}_b/\hbar}|\Psi(\mathbf{r}_b,\mathbf{r}_c)\rangle|^2 , \tag{3.16}$$

where $-\mathbf{q}$ is the recoil momentum of the residual ion resulting from the ejection of the target electron and is equal to the difference between the momentum of the incident electron and the momenta of the scattered and ejected electrons. For momentum to be conserved, this recoil momentum is equal in magnitude and opposite in direction to the momentum of the ejected electron at the instant of ejection. Returning to Eq. (3.16), we note that the factor $4m^2e^4/\hbar^4K^4$ is the Rutherford cross section for electron-electron scattering and has units of area. The second factor $k_a k_b/k_0$ is a flux term that accounts for the different fluxes of the incident, scattered, and ejected electrons and has units of momentum divided by $\hbar$. The last factor

$$|\langle\Phi_{i\alpha}(r_c)|e^{i\mathbf{q}\cdot\mathbf{r}_b/\hbar}|\Psi(\mathbf{r}_b,\mathbf{r}_c)\rangle|^2$$

has the units of momentum density, or the reciprocal of momentum cubed. In nuclear physics this factor is called the *form factor* and is a measure of the deviation of the target from a point. Taken together, the three factors have units of area divided by momentum squared or area over energy. Because of the indistinguishability of electrons, Eq. (3.16) should be modified to take into account exchange. This effect is largest for symmetric geometries in which the energies of the scattered and ejected electrons are identical. In the dipole region where momentum transfer approaches zero, the Rutherford and exchange cross sections are nearly identical. It is also important to note that the first factor depends only on the coordinates of the incident electron, while the momentum density factor is only a function of the internal coordinates of the target and residual ion. This separation provides the operational basis of $(e,2e)$ spectroscopy because the part of the cross section that depends on the properties of the target can be isolated from the part as-

sociated with the collision. The separation is called *factorization* and can be experimentally tested through the measurement of momentum density for different values of momentum transfer. Since momentum density is a property of the target, it should be invariant with momentum transfer if the factorization approximation is valid.

The matrix element (3.16) has a particularly simple interpretation if the initial-target wave function and residual-ion wave functions can each be represented by a single-orbital-product function. Let us consider the case in which

$$\Psi(\mathbf{r}_b,\mathbf{r}_c)=\psi_b(\mathbf{r}_b)\psi_c(\mathbf{r}_c),\quad \Phi_{bc}(\mathbf{r}_c)=\phi_c(\mathbf{r}_c)\ . \tag{3.17}$$

The integrations over $\mathbf{r}_b$ and $\mathbf{r}_c$ in the expression for the matrix element give the product of the overlap of $\phi_c(\mathbf{r}_c)$ and $\psi_c\mathbf{r}_c$ and the Fourier transform of $\psi_b(\mathbf{r}_b)$,

$$\langle\phi_c(\mathbf{r}_c)|\psi_c(\mathbf{r}_c)\rangle\int e^{i\mathbf{q}\cdot\mathbf{r}_b/\hbar}\psi_b(\mathbf{r}_b)d\mathbf{r}_b\ . \tag{3.18}$$

The square of the absolute value of the first term is called the *spectroscopic factor,* and the square of the absolute value of the integral on the right is the square modulus of the single-electron wave function in q space—*the momentum density* $\rho(\mathbf{q})$. The integral of $\rho(\mathbf{q})$ over the volume $\sin(\theta)\cos(\phi)q^2d\theta\,d\phi\,dq$ is unity.

The *frozen-core approximation,* a further simplification, is based on treating the occupied orbitals of the ion as identical to the corresponding orbitals in the neutral atom. In this approximation, $\phi_c(\mathbf{r}_c)=\psi_c(\mathbf{r}_c)$, the spectroscopic factor is unity, and the matrix element equals the momentum density directly. The frozen-core approximation is also called the *sudden approximation,* the name based on the assumption that the ejected electron leaves the atom in a time much less than the time it takes for the remaining electrons to adjust their motion to absence of the ejected electron.

It is often observed that the ejection of an electron by an incident electron results in the simultaneous excitation of a second electron, leaving the residual ion in a state above the single-hole state. This phenomenon occurs through the correlated motion of the electrons in the target and reflects the inadequacy of single-electron-product wave functions that assume independent motion of the bound electrons. One method for accounting for correlation is to use a *configuration interaction* (CI) wave function. A CI wave function is written as a linear combination of single-electron-product wave functions. For the residual ion, these functions include a representation of the single-hole state arising from simple ejection of the target electron as well as multiple-hole states arising from the ejection of one electron and the simultaneous excitation of one or more other electrons. For the target, the CI wave function includes a representation of the ground state as well as excited states of the same symmetry. For the case of molecules, the target is almost always a closed-shell system, and electron correlation is thus frequently more important in the open-shell ion. In this event, a CI wave function is only used to represent the final states of the $(e,2e)$ reaction, and the functional proportionality between the cross section and the target-electron momentum density can be retained.

The main features of the various theoretical scattering treatments are summarized in Table I. Figure 5 is a graphical representation of the kinematics of electron impact and contains much of the information in Table I in a different form. The allowed values of momentum transfer, $\hbar K$ (in units of the electron momentum of the first Bohr orbit) for a range of incident-electron energies E_0 (in units of twice the ionization potential of hydrogen), at a single incident-electron energy loss of 27.2 eV, are bounded by the single curved line. The upper half of the curve corresponds to a scattering angle of 180°, while the lower half is for 0° scattering. The region around $\hbar K=1$ a.u. is the *threshold* region, where the energies of the scattered and ejected electrons are small and the Coulomb interactions between the scattered and ejected electrons and the residual ion core dominate. *Binary* collisions, in which energy lost by the incident electron is completely transferred to a target electron, correspond to the horizontal line at a $\hbar K$ value of 1 a.u. This is the region of the Bethe ridge shown in Fig. 3. At large values of momentum transfer, the incident electron interacts with the target core as well as with the target electron. This interaction can be accounted for with the *second Born approximation.* At sufficiently high incident-electron energies where the incident and scattered electrons can be represented by plane waves, and interaction with the core is small, the first Born approximation is the appropriate theory. The *first-Born-approximation* region overlaps the *dipole* region, where the incident electron can be treated very much like a photon. At intermediate values of incident energy and momentum transfer all of the interactions between the electrons and core are of comparable strength, and various distorted wave theories are needed to accurately describe the scattering.

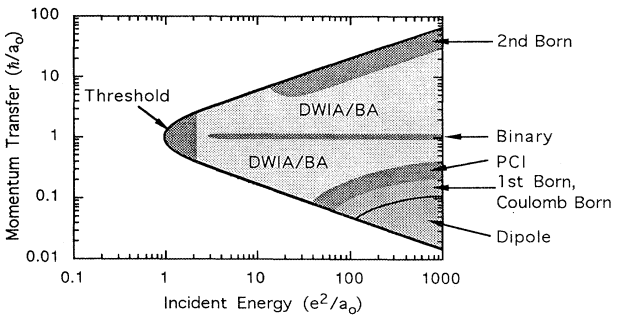

FIG. 5. Coexistence diagram showing the allowed values of momentum transfer $\hbar K$ for a range of incident-electron energies. The energies are in units of twice the ionization potential of hydrogen (e^2/a_0). The energy loss is fixed at 27.2 eV. The threshold, dipole, and binary regions are shown along with the regions where the first-Born, second-Born, distorted-wave impulse (DWIA), and post-collision interaction (PCI) approximations are applied.

D. Comparisons between theory and experiment

As we pointed out before, there are two distinct branches of electron-impact ionization research. Both were started at about the same time and continued up to only a few years ago with comparatively little overlap. This review is concerned with the determination of momentum densities by electron-impact ionization, but there is much to be learned from the experiments and theories that are mostly concerned with the nature of ionization. While the formalism is identical for the two different lines of research, the kinematic regimes can be very different. Since we are still very far from a universal theory of electron scattering, the kinematics of a particular experiment dictate the appropriate theory. In this section we will briefly review the research on ionization and then concentrate on the theories and experiments most often used for momentum-density determinations.

1. Ionization mechanism

The first electron-impact ionization experiments with full determination of the angles and energies of the scat-

TABLE I. (e,2e) theoretical treatments.

Interaction	Projectile electron (e_p)	Target electron (e_t)	Ejected electron (slow)	Scattered electron (Fast)	Approximation	Reference
e_p-e_t	Plane wave	Target state	Plane wave	Plane wave	PWBA	Glassgold and Ialongo (1968)
e_p-e_t	Plane wave	Target state	Coulomb wave	Plane wave	1st Born	Joachain and Piraux (1986)
Asymptotic 3-body Coulomb	Plane wave	Target state	Coupled asymptotic		BBK	Brauner *et al.* (1989)
e_p-e_t e_p-target	Plane wave	Target state	X^+, Second-order perturbation		2nd Born	Byron, Joachain, and Piraux (1986)
All orders	Plane wave	Target state	X^+ solution of close coupling equations		Pseudostates includes all interations	Mota Furtado and O'Mahony (1989)
e_p-e_t	Plane wave	Target state	Coulomb wave	Coulomb wave	Coulomb projected Born with exchange	Geltman (1974)
e_p-e_t	Wave in static exchange potential of the atom	Target state	Wave in static exchange potential of the ion	Wave in static exchange potential of the ion	DWBA (Asymmetric)	Zhang *et al.* (1992)
e_p-e_t	Wave in static exchange potential of the atom	Target state	Wave in static exchange potential of the ion	Wave in static exchange potential of the ion	DWBA (Symmetric)	Zhang *et al.* (1990a)
e_p-e_t	Wave in optical potential of the atom	Target state	Wave in optical potential of the ion	Wave in optical potential of the ion	DWIA	McCarthy and Weigold (1976)
e_p-e_t	Plane wave	Target state	Wave in the Coulomb potential of the scattered electron	Wave in the Coulomb potential of the ejected electron	PCI	Popov and Erokhin (1983)
e_p-e_t	Wavelength adjusted plane wave	Target state	Plane wave	Plane wave	Eikonal	Camilloni *et al.* (1978)

tered and ejected electrons were done by Ehrhardt *et al.* at an incident energy of 500 eV on helium (Ehrhardt *et al.*, 1969, 1972a, 1972b, 1982a; Jung *et al.*, 1985). The scattered electron was detected at a fixed, small angle with respect to the incident direction, and the ejected electrons were detected in coincidence with the scattered electron over a wide angular range in the plane of the incident and scattered electron. This is the *asymmetric*-coplanar geometry. Under these conditions, the ejected electrons were mostly concentrated in an angular range about the momentum-transfer direction. Ejected electrons were also detected over a range of angles in the direction opposite to the momentum-transfer direction. This is illustrated schematically in Fig. 6. The ejected electrons in the forward direction were called *binary electrons,* and those in the backward direction *recoil electrons.* The general features of the experiments were explained by a model in which two different types of scattering take place. The first is direct electron-electron scattering giving rise to the binary lobe. The second is an electron-electron collision followed by scattering of the target electron from the ion core to produce the recoil lobe. Once the basic nature of the collision was understood, most of the theoretical effort was directed toward calculating the details of the direction, shape, and magnitude of the binary and recoil lobes. The calculations have been done at a variety of levels of approximation. The simplest uses plane waves for the incident and scattered electrons with a Coulomb wave for the ejected electrons (Ehrhardt *et al.*, 1982b). More complex calculations were based on the distorted-wave formalism (Madison *et al.*, 1977; Bransden *et al.*, 1978) and the second Born approximation (Byron *et al.*, 1980; 1982). Generally, the more complex theories predict the position of the binary peak and the ratio of binary to recoil peak intensities to within 20% of the observations. There has been less success calculating the position of the recoil peak. It was not possible to ascertain from these results whether the remaining discrepancies were due to inadequacies in the formulation of the collision process or deficiencies in the target wave function. To remove questions concerning the target wave function, Ehrhardt *et al.* (1985) performed a series of experiments on atomic hydrogen at incident energies of 250, 150, and 54.4 eV.

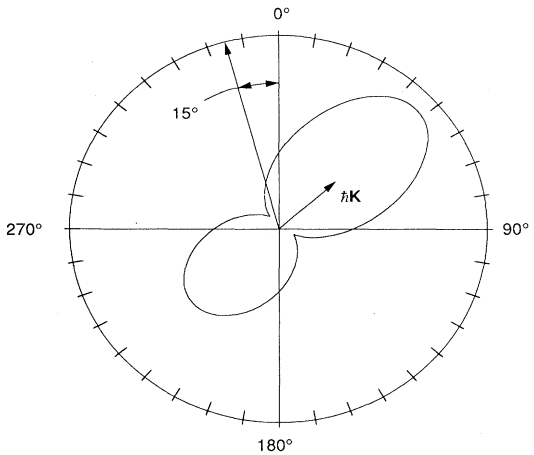

FIG. 6. Schematic diagram of scattering at intermediate momentum transfer. The direction of scattering of the incident electron is shown along with the momentum-transfer direction. The two lobes show the relative magnitude and direction of the ejected electrons. The lobe in the forward direction is the binary lobe. It is associated with the direct knockout of the target electron. The lobe in the backward direction is the recoil lobe. It is a result of the collision of the ejected electron with the residual-ion core.

The first series of $(e,2e)$ experiments have been followed by experiments that cover an expanded range of kinematic parameters. There are now also a number of absolute $(e,2e)$ cross-section measurements in the coplanar-asymmetric geometry in which the scattered electron has lost only a small fraction of its incident energy and the ejected electrons have energies at most a few times their binding energies. Avaldi *et al.* (1992) have made measurements on helium for incident-electron energies of 300 eV and ejected-electron energies of 10 and 18.4 eV. At incident energies of 100 and 200 eV there are also the absolute data of Cherid *et al.* (1992). At higher energies there are the 8 keV measurements of Daoud *et al.* (1985) on neon, the helium measurements of Avaldi *et al.* (1987b) at 1024.6 eV, Duguet *et al.* (1987) at incident energies of 4 and 8 keV, and the measurements of Lahmam-Bennani *et al.* (1988) at 0.5, 1.5, and 8 keV. Lahmam-Bennani has discussed the different procedures for establishing an absolute scale for the higher-energy, asymmetric experiments (Lahmam-Bennani *et al.*, 1987). The methods depend essentially on the applicability of the Born approximation and extrapolation to the optical limit.

Early, absolute, nonsymmetric measurements were made by Beaty *et al.* (1977) on helium and by Stefani *et al.* (1978, 1979) on helium and neon. Van Wingerden *et al.* (1979) measured the absolute value of the $(e,2e)$ cross section at 45° in the symmetric-coplanar geometry. More recently Pochat *et al.* (1987) have made absolute measurements of the triply differential cross section in the symmetric geometry over a range of angles at an incident energy of 200 eV. The measurements were extended to large momentum transfer and large recoil momenta. Improved measurements in this geometry at 200 eV have been made by Frost *et al.* (1990) and Gélébart *et al.* (1990). These have been followed by measurements at 100 eV (Gélébart and Tweed, 1990). The absolute scale for the measurements has been established by reference to absolute, elastic-scattering cross sections.

Absolute symmetric measurements have been compared with a variety of calculations. McCarthy and Roberts (1987) have compared plane-wave impulse approximation calculations with the data of van Wingerden *et al.* (1979) and found good agreement. Data at 100 eV (Gélébart and Tweed, 1990), and 200 eV (Gélébart *et al.*, 1990) are not in agreement with the van Wingerden

et al. (1979) data, but there is reasonable accord with distorted-wave Born-approximation (DWBA) calculations (Zhang *et al.* 1990a; Cherid *et al.*, 1992).

Triple-differential cross section data have also been extended to hundreds of kilovolts in which relativistic effects begin to be important (Schröter *et al.*, 1990; Schüle and Nakel, 1982; Walters *et al.*, 1992). At the higher energies, inner-shell ionization has been investigated for silver and tantalum (Ruhoff and Nakel, 1987).

Though most experiments continue to use the coplanar geometry, a series of experiments have been done in the out-of-plane geometry, in which the ejected electron is detected in a plane that lies at a large angle with respect to the plane of the incident and scattered-electron wave vectors. Out-of-plane kinematics preferentially select ionizing collisions in which a strong electron-core interaction has occurred. Cvejanovic and Read (1974) have done out-of-plane experiments with the plane of the detected electron at 150° and 180° to the plane of the incident and scattered electrons. The energies of the detected electrons were 0.2 to 0.3 eV above threshold. Jones *et al.* (1990) have measured the angular distribution of 1 and 2 eV electrons as a function of the out-of-plane angle and Rösel *et al.* (1982) have made absolute measurements in the perpendicular plane at 2 eV above the threshold for the ionization of helium. Distorted-wave Born-approximation calculations for this geometry have been remarkably successful in reproducing the experimental results (Zhang *et al.*, 1990a).

Experiments with polarized targets (Frost *et al.*, 1990) have been done, and there are calculations of $(e,2e)$ cross sections in intense laser fields (Joachain *et al.*, 1988; Martin *et al.*, 1989).

2. Momentum densities

The practical determination of momentum densities requires that there be a straightforward relation between the $(e,2e)$ cross section and momentum density. The plane-wave impulse approximation (PWIA) meets this requirement, but it is essential that the various assumptions of the theory be tested experimentally if it is to be used to get reliable results.

The approximation that the incident electron interacts only with the target electron and that all other interactions can be ignored (impulse approximation) is expected to be valid for target electrons in the valence shell, and can be tested by comparing the absolute cross-section measurements with impulse approximation calculations. As expected, the results show attenuation of the scattered and ejected electrons at low incident-electron energies. Generally, the impulse approximation is reliable for impact energies ten to one hundred times the binding energy of the target electron. Correspondingly, the energies of the scattered and ejected electrons should also be of this order of magnitude for the impulse approximation to be useful.

Factorization can be experimentally tested by measuring the $(e,2e)$ cross section as a function of q for different values of $\mathbf{K}$. Since $\mathbf{K}$ is essentially a scale factor, $d^3\sigma_{(e,2e)}/d\Omega_a d\Omega_b dE_b$ should only depend on the square of the magnitude of the matrix element

$$|\langle \Phi_{i\alpha}(\mathbf{r}_c)|e^{i\mathbf{q}\cdot\mathbf{r}_b/\hbar}|\Psi(\mathbf{r}_b,\mathbf{r}_c)\rangle|^2 , \tag{3.19}$$

which is independent of $\mathbf{K}$. For the case of an N-electron target and an $(N-1)$-electron residual ion, the simple product wave functions have the form

$$\Psi=\frac{1}{\sqrt{N}}\sum_{l=1}^{N} a_l\psi_l(\mathbf{r}_l) ,$$

$$\Phi_{i\alpha}=\frac{1}{\sqrt{N-1}}\sum_{m=1}^{N-1} b_m\phi_m(\mathbf{r}_m), \quad m\neq i .$$

The degree of correctness of the electron-electron term in the expression for the $(e,2e)$ cross section can be ascertained through measurements in which q is held constant and only $\mathbf{K}$ varied. Early tests of the validity of factorization were done by Hood *et al.* (1973). These were followed by detailed experiments in both coplanar and noncoplanar geometries by Camilloni *et al.* (1978) and Giardini-Guidoni *et al.* (1980). The results of the experimental tests have shown that for symmetric kinematics and large values of $\mathbf{K}$, of the order of several times $\hbar/a_0$, the shape of the $(e,2e)$ cross section is independent of $\mathbf{K}$ so long as the magnitude of q does not exceed approximately two times $\hbar/a_0$.

It is important to note that a large-momentum-transfer collision in which the incident electron loses most of its energy is not equivalent to a collision with the same momentum transfer in which the scattered and ejected electrons leave the collision with substantial energies. In the first case, the wave function of the low-energy scattered electron cannot be accurately described by a plane wave. For this reason $(e,2e)$ spectroscopy is best carried out at large momentum transfer and large scattered and ejected-electron energies. This can be achieved with symmetric kinematics in which the incident electron gives up half of its momentum to the target electron and the scattered and ejected electrons each have the same momentum. The symmetric-noncoplanar geometry will be discussed in more detail in the experimental section. It satisfies the conditions for the validity of the PWIA, but is limited by the fact that the triple-differential cross section is a minimum at the polar angles normally used. To overcome this problem a number of other geometries have been proposed. The potentially most useful is the coplanar-asymmetric geometry with incident-electron energies from one to several keV and ejected-electron energies as low as 100 eV (Lahmam-Bennani *et al.*, 1983; Daoud *et al.*, 1985; Avaldi *et al.*, 1987a). Momentum densities derived from the asymmetric measurements for nitrogen are in good agreement with those obtained in the symmetric-noncoplanar geometry, and there is the advantage of shorter data collection times. This geometry also allows for the measurement of absolute momentum densities.

Extensions of the PWIA have been tried in an effort to expand the region of applicability of the theory. The eikonal approximation is very much like the PWIA and preserves the separation of collision and structure terms (Stefani and Camilloni, 1985). The factorized, distorted-wave approximation goes one step farther. In this extension of the plane-wave impulse approximation the incident-, scattered-, and ejected-electron waves are calculated in an optical potential that depends only on the distance between the electrons and the core (Dixon *et al.*, 1978; Fuss *et al.*, 1978, Weigold *et al.*, 1979). A consequence of using distorted rather than plane waves is that we no longer preserve the simple interpretation of the structure factor as the square of the Fourier transform of the one-electron wave function. Instead, the transform is now a distorted-wave transform, a function that is more difficult to interpret.

IV. EXPERIMENTAL METHODS

A. General considerations

Determination of momentum densities from $(e,2e)$ processes requires an experimental regime in which the scattering dynamics can be described quantitatively and the ionization cross section is sufficiently large to provide an adequate signal-to-noise ratio. Current practice is to work at high incident energies and large momentum transfer so that the expression for the cross section can be factored into the product of a term that depends on the scattering geometry and a term containing the momentum density of the target electron [Eq. (3.16)]. Scattering geometries are chosen so that the scattering term is either constant or varies slowly, in a predictable manner, with the independent variable. Unfortunately, the requirement for an accurate theoretical description of the scattering dynamics obliges experimenters to work under conditions in which the ionization cross section is at, or near, its minimum value.

The experiments are carried out in high vacuum using standard cathode-ray-tube (CRT)-type electron guns with thermionic cathodes as sources and (in most cases) electrostatic-deflection analyzers with electron multipliers to detect the outgoing electrons. Nanosecond timing electronics are used and, since measurement of the momentum density for a single orbital may require a day or more, long-term stability in the entire system is essential. Electron trajectories must be measured with an accuracy of a fraction of one degree; magnetic shielding is required to reduce the ambient field to a milligauss or less. The energy of the outgoing electrons is usually measured with a resolution consistent with the energy width characteristic of the source, 0.5 to 1.0 eV [full width at half maximum (FWHM)], by using decelerating lens systems between the target volume and the energy analyzers of the outgoing electrons.

Two types of data can be collected in an $(e,2e)$ spectroscopy experiment: the momentum density as a function of momentum for a particular orbital (identified with a particular ionization potential, IP), and the momentum density at a fixed momentum value as a function of IP (a binding-energy or separation-energy spectrum). The former is scanned by sweeping the independent variable identified in Table II; the latter is scanned by holding the independent variable fixed and sweeping the incident energy. The binding-energy spectrum serves not only to identify the energies of ionization processes in the target atom or molecule (in a manner similar to photoelectron spectroscopy), but, depending on the selection of momentum, helps identify the symmetry of the orbital from which an electron is ejected. For example, only orbitals containing a totally symmetric component (i.e., atomic s orbitals or molecular σ_g orbitals) will have a significant momentum density near $q=0$, whereas orbitals of lower symmetry often have nodes at $q=0$ with the largest momentum densities near $q=0.5\hbar/a_0$.

B. Source and detector configurations

The geometry of an $(e,2e)$ experiment can be described in terms of the variables E_0, E_a, E_b, θ_a, θ_b, and ϕ defined in Fig. 1. The various scattering apparatus geometries are summarized in Table II. In the plane-wave impulse approximation expression for the $(e,2e)$ cross section (3.16), the scattering term is nearly constant if the momentum transfer $\hbar\mathbf{K}$ is fixed. This can be accomplished in a geometry in which the incident-electron energy, the scattering angle, and the energy loss do not change, that is, where E_0, E_a, and θ_a are fixed. The PWIA is most accurate when $\mathbf{K}$ is large, a condition that is best met with symmetric sharing of energy between the outgoing electrons so that $E_a=E_b$. Under these conditions an initially stationary, unbound target electron would be ejected in the plane defined by $\mathbf{k}_0$ and $\mathbf{k}_a$, with $\theta_a=\theta_b=45°$. For an actual target electron in a bound orbital, the initial momentum adds to that of a stationary target. The ejected electron may move out of the plane defined by the incident and scattered directions so that the azimuthal angle ϕ is different from zero. The value of ϕ, or the derivation of θ_b from 45°, is a measure of the initial momentum of the target electron.

The great majority of $(e,2e)$ momentum-density determinations have been carried out in the symmetric-noncoplanar geometry wherein ϕ is chosen as the independent variable. In this geometry the incident-electron energy is fixed at an energy two to three orders of magnitude greater than the binding energy of the target electron, and scattering events are selected in which the available post-collision energy is symmetrically shared between the outgoing electrons ($E_a=E_b=E=(E_0-IP)/2$). The polar angles describing the trajec-

TABLE II. Summary of geometries used in $(e,2e)$ spectroscopy experiments.

Geometry	Constraints (experimental parameters held constant)	Independent variable	Target momentum q	Typical range of parameters[a]	Apparatus reference
Symmetric-noncoplanar	$E_a=E_b=\frac{E_0-IP}{2}=E$ $\theta_a=\theta_b=\theta$	ϕ	$2\sqrt{2}\left[\left[\sqrt{E}\cos\theta-\frac{\sqrt{E_0}}{2}\right]^2+E\sin^2\theta\sin^2\frac{\phi}{2}\right]^{1/2}$	E_0=400–2000 eV θ=45°	McCarthy and Weigold (1976) Minchinton *et al.* (1982) Weigold (1990) Hood *et al.* (1977) Leung and Brion (1983) Banjavcic *et al.* (1991) Moore *et al.* (1978) Goruganthu *et al.* (1988) Leung (1991)
Symmetric-coplanar	$E_a=E_b=\frac{E_0-IP}{2}=E$ $\phi=0$	$\theta=\theta_a=\theta_b$	$2\sqrt{2}\left[\left[\sqrt{E}\cos\theta-\frac{\sqrt{E_0}}{2}\right]^2\right]^{1/2}$	E_0=400–2600 eV θ=30–60	Camilloni *et al.* (1978) Camilloni *et al.* (1972) Ritter, Dennison, and Dunn (1984)
Out-of-plane symmetric	$E_a=E_b=\frac{E_0-IP}{2}=E$ $\theta'=\theta'_a=\theta'_b$ (scattering angle in plane of outgoing electrons) $\cos\theta\cos\phi=D(=\cos\theta')$	$\phi'=\arcsin\left[\left[\frac{\sin\theta}{\cos\theta}\right]\sin\frac{\phi}{2}\right]$ (elevation of incident electron direction above plane of outgoing electrons)	$2\sqrt{2}\left[\left[\sqrt{E}\frac{D}{\cos\phi'}-\frac{\sqrt{E_0}}{2}\right]^2+ED^2\tan^2\phi'\right]^{1/2}$	E_0=800–2600 eV θ=44–45° ϕ=0–8°	Fantoni *et al.* (1980) Giardini-Guidoni *et al.* (1978) Ritter, Dennison, and Dunn (1984)
Highly asymmetric	$E_a \gg E_b$	θ_b	$2\left[\begin{array}{l}\left[E_0-\frac{IP}{2}\right]\\+\sqrt{E_aE_b}(\cos\theta_a\cos\theta_b-\sin\theta_a\sin\theta_b\cos\phi)\\-\sqrt{E_0}(\sqrt{E_a}\cos\theta_a+\sqrt{E_b}\cos\theta_b)\end{array}\right]^{1/2}$	E_0=8000 eV	Lahmam-Bennani *et al.* (1985)
coplanar	θ_a (small) θ_a (small) $\phi=0$			E_b=400–600 eV θ_a=10–17 eV θ_b=30–140°	
Nonsymmetric-coplanar (coplanar energy-sharing)	$E_0=E_a+E_b+IP$ $\theta_a+\theta_b=\theta$ $\phi=0$	$\Delta E=E_a-E_b$	$\sqrt{2}\left[\begin{array}{l}2E_0-IP\\+\sqrt{(E_0-IP)^2-\Delta E^2}(\cos^2\theta-\sin^2\theta)\\-\sqrt{2E_0}(\sqrt{E_0-IP+\Delta E}+\sqrt{E_0-IP-\Delta E})\cos\theta\end{array}\right]^{1/2}$		Lower *et al.* (1991)

tories of the scattered and ejected electrons are equal ($\theta_a = \theta_b = \theta$) and set at 45°. The simple monotonic relation between ϕ and the target electron momentum $\mathbf{q}$ in the symmetric noncoplanar geometry is given in Table II. It is worth noting that, since IP is always finite, zero on the momentum scale is inaccessible when $\theta = 45°$.

Electron momentum densities have been derived from experiments carried out in other geometries as indicated in Table II. The first $(e,2e)$ spectroscopy experiment (Camilloni *et al.*, 1972) employed a symmetric coplanar arrangement in which the polar scattering angle ($\theta_a = \theta_b = \theta$) was varied while the azimuthal angle ϕ was fixed at zero. This geometry provided experimental simplicity; however, the interpretation of data is more difficult than for the symmetric-noncoplanar case since the $(e,2e)$ cross section in the former geometry is very sensitive to the scattering approximation (Camilloni *et al.*, 1978). The accuracy of interpretation in these experiments was improved by turning to an "out-of-plane" symmetric geometry in which the detectors for the scattered and ejected electrons remain stationary relative to the scattering center so that the scattered and ejected-electron trajectories define a plane, and the position of the incident electron source was moved (Giardini-Guidoni *et al.*, 1978; Fantoni *et al.*, 1980). The independent variable was the angle of elevation, ϕ', of the electron source relative to the plane defined by the two detectors and the scattering source. In this geometry the scattering angle θ_a, and hence the momentum transfer, are only weak functions of ϕ', and, furthermore, the data appear to be less sensitive to distortion effects (Camilloni *et al.*, 1980).

The $(e,2e)$ cross section increases as the scattering geometry becomes asymmetric; however, this increase comes at the expense of a decrease in momentum transfer for a fixed incident energy. Momentum densities have been obtained in a highly asymmetric coplanar geometry by using an incident energy greater than that used in symmetric experiments to insure that the momentum transfer was sufficiently large to ensure the validity of the plane-wave impulse approximation. So long as the kinematic conditions correspond to those of the Bethe ridge (see Fig. 3), accurate momentum densities can be extracted from the scattering data (Avaldi *et al.*, 1987a).

Recently $(e,2e)$ spectroscopy measurements have been carried out using a geometry in which all the scattering angles are held constant and the momentum spectrum is scanned by varying the distribution of energy between the two outgoing electrons (Lower *et al.*, 1991). This geometry is nonsymmetric coplanar ($\theta_a = \theta_b$), and the independent variable is $\Delta E = E_a - E_b$. The advantage of such an experiment is that there are no moving parts. The momentum density is scanned by varying electrical potentials. The disadvantage is that the value of the momentum transfer changes as the momentum spectrum is scanned, and this variation must be accurately accounted for when extracting a momentum density from the measured cross sections.

C. Coincidence techniques and signal-to-noise considerations

In an $(e,2e)$ experiment, pairs of electrons are detected in such a way as to be certain that they both originated from a single ionization event. This is accomplished through a determination of the arrival times of the electrons at the detectors. In principle, the arrivals of two $(e,2e)$ electrons is precisely correlated in time (in a symmetric experiment there is a zero time difference between the arrivals of the two electrons). Asymmetries in velocities and path lengths and delays in the measuring electronics introduce an unavoidable dispersion in the arrival time. This dispersion establishes the time resolution $\Delta\tau$ of the experiment. Figure 7 is an example of a time spectrum in which the number of two-electron detection events is plotted as a function of the difference between arrival times. For convenience, perfect coincidence, corresponding to zero time difference, is made to appear in the center of the spectrum by inserting a delay into the electronic path from one of the detectors. The coincidence counts appear on a background that arises from separate events that accidentally occur with the same time correlation as true coincidences. The $(e,2e)$ signal is therefore the total number of events in the coincidence window ($N_C + N_A$) minus the number of accidental coincidences in the window (N_A). This latter quantity cannot be determined directly, but is inferred from the number of accidental coincidences adjacent to the coincidence window. The relative statistical uncertainty in

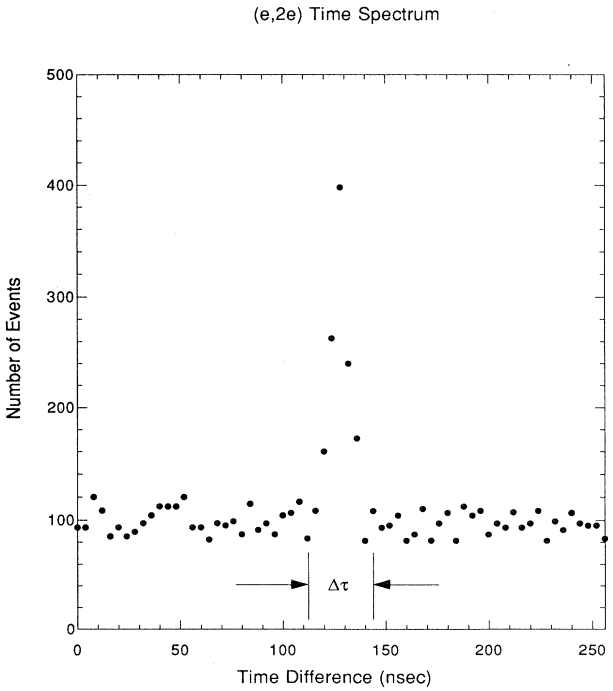

FIG. 7. Arrival time spectrum for one outgoing electron relative to the second electron.

an (e,2e) measurement can be estimated as $\sqrt{N_C+2N_A}/N_C$, where the uncertainties in the total counts and accidental counts have been added in quadrature.

In order to understand the limitations and advantages of the coincidence technique, it is useful to obtain expressions for the signal and the statistical uncertainty in terms of the experimental parameters and relevant cross sections. We begin with expressions for the true and accidental coincidence rates, R_C and R_A.

The true coincidence rate (R_C) depends upon the cross section for electron-impact ionization ($d^4\sigma_{(e,2e)}/d\Omega_a d\Omega_b dE_a dE_b$), the incident electron current I_0, the target density n and length l, and the instrument parameters that determine the resolution of the experiment ($\Delta E_a, \Delta E_b, \Delta\Omega_a, \Delta\Omega_b$):[2]

$$R_C = I_0 nl (d^4\sigma_{(e,2e)}/d\Omega_a d\Omega_b dE_a dE_b) \times \Delta E_a \Delta E_b \Delta\Omega_a \Delta\Omega_b \ . \quad (4.1)$$

The rate of accidental coincidences within a time window $\Delta\tau$ is given by the product of the accidental count rate at each detector (the singles rate) and $\Delta\tau$. The singles rate at each detector depends on the cross section for ejection of an electron into the detector, the incident current, the target density and length, and the energy and angle resolution of each detector. Assuming the electrons contributing to the singles counts originate only in the scattering volume, these are the cross sections σ_a and σ_b for the ejection of electrons of nominal energy E_a or E_b integrated over the energy and solid angle of the scattered electron. The accidental coincidence rate is

$$R_A = (I_0 nl \sigma_a \Delta E_a \Delta\Omega_a)(I_0 nl \sigma_b \Delta E_b \Delta\Omega_b)\Delta\tau \ . \quad (4.2)$$

The accidental rate will be increased if singles that originate from other processes, such as scattering from electrode surfaces, enter the detectors. It is essential that the detectors be shielded from stray electrons. Unwanted stray electrons can be effectively excluded by baffles between the scattering volume and the electron energy analyzers, by isolating the electron gun in a separate, differentially pumped chamber, and by surrounding the entire apparatus with a positive-biased screen to collect slow stray electrons (Goruganthu *et al.*, 1988). Multiple-scattering effects, endemic to transmission (e,2e) experiments on solid films, have been compensated for by deconvolution techniques (Jones and Ritter, 1986).

For a total data collection time t, the number of true coincidences will be $R_C t$ and the number of accidental coincidences will be $R_A t$. The relative statistical uncertainty of an (e,2e) measurement over a given period of time (t) is

$$\sqrt{\mu} = \frac{\sqrt{R_C+2R_A}}{R_C t^{1/2}} \ . \quad (4.3)$$

This quantity can be decreased by increasing the incident current or the target density; however, beyond a certain point, the advantage of this approach diminishes rapidly because the number of accidental coincidences increases as the square of $I_0 nl$. Typical (e,2e) experiments are carried out in a regime where R_C/R_A approaches unity. In this case the relative statistical uncertainty approaches $\sqrt{\frac{2}{3}}$ of its value at the high-current/high-density limit.

The precision of an (e,2e) experiment is improved by reducing the accidental coincidence rate. This is usually accomplished by reducing the coincidence time window ($\Delta\tau$). Schemes have recently been put forward to deal with the variation in flight times of electrons through electric-deflection energy analyzers (Volker and Sandner, 1983; Best and Zhu, 1985; Hayes *et al.*, 1988; Lower and Weigold, 1989). Fast rise-time amplifiers and constant-fraction discriminators can be used to reduce electronic time dispersion. The statistical uncertainty in the determination of N_A can be reduced by measuring the accidental rate over time windows that are much wider than Δt and scaling the results by the ratio of the window width to Δt. The corresponding reduction in accidental rate uncertainty is the square root of this ratio.

D. Momentum-space resolution

The resolution in momentum space is significantly limited by the experimental conditions necessary to give a statistical uncertainty adequate to permit meaningful comparisons between experimentally-obtained momentum densities and theoretical calculations. Incident currents are up to 10 μA, the maximum obtainable from a well-collimated electron source without serious degradation of the energy width. Gas-phase experiments are carried out with a target pressure of about 1 mtorr; a greater target pressure would result in a significant number of multiple-scattering events. The typical timing resolution of 3–5 ns is established by the dispersion of flight times through the electron analyzers rather than by the resolution of the timing electronics. The magnitude of the cross sections that appear in the expressions for R_C and R_A is determined by the choices of incident-electron energy and scattering geometry needed to allow accurate interpretation of the experimental data The energy resolution of the experiment is established by the energy width characteristic of the electron gun. Typical data collection times for each point on the momentum density are of the order of 1 to 10 h (see, however, Gao *et al.*, 1988). Because of the weak dependence of $\sqrt{\mu}$ on t, it is impractical to increase the data collection time in order to improve the precision of the data significantly. An increase in the angular acceptance of the detectors ($\Delta\Omega$) decreases $\sqrt{\mu}$; however, the resolution in momen-

[2]Overall energy resolution can be approximated by $\Delta E_a \Delta E_b$ or more accurately by the sum in quadrature subject to energy conservation as discussed by Lahmam-Bennani *et al.* (1985).

tum space is almost exclusively determined by the angular resolution. In the most recent experiments under the conditions described in Table II a statistical uncertainty of 3% is obtained with angular resolution of about 3×10^{-4} sr. Under these conditions the momentum resolution is $0.07-0.10\ \hbar/a_0$.

E. Multiplexed experiments

A number of innovations have led to significant improvements in both the precision and accuracy of $(e,2e)$ spectroscopy. The most important are schemes that permit many $(e,2e)$ measurements to be carried out simultaneously. Moore and co-workers (Moore *et al.*, 1978; Goruganthu *et al.*, 1988) have developed a symmetric-noncoplanar apparatus, illustrated in Fig. 8, that uses a single spherical electrostatic energy analyzer to select the energies of both outgoing electrons. An array of electron multipliers in the exit plane of the analyzer are arranged so that each pair of detectors corresponds to a different azimuthal angle (ϕ) and hence to a different value of momentum of the target electron. A multiplexed timing circuit permits coincidences at every pair of detectors to be monitored simultaneously (Skillman *et al.*, 1978; Goruganthu *et al.*, 1988). As many as 49 points on the momentum density can be measured at once. Weigold and co-workers (Cook, McCarthy, Stelbovics, and Weigold, 1984; Cook, Mitroy, and Weigold, 1984; Lower and Weigold, 1989; Weigold, 1990) and Williams and his collaborators (Hayes *et al.*, 1988) have taken a different approach by developing a multiplexed apparatus that permits an entire binding energy spectrum to be observed at a single value of momentum. This apparatus uses two spherical, electrostatic-deflection-type energy analyzers in a symmetric-noncoplanar geometry. Scattered electrons are dispersed in energy across multichannel-plate position-sensitive detectors at the output focal plane of each analyzer.

F. Solids

In spite of the fact that the first experiments were performed on the carbon K-shell electrons in carbon-containing solid films (Amaldi *et al.*, 1969; Camilloni *et al.*, 1972), $(e,2e)$ spectroscopy of solids has not progressed nearly so far as work on isolated gaseous atoms and molecules. Daunting technical difficulties are no doubt the reason for this lack of progress. Early work on K- and L-shell electrons of carbon in evaporated carbon and hydrocarbon films (Krasil'nikova *et al.*, 1975) and of aluminum in polycrystalline aluminum (or aluminum oxide; Persiantseva *et al.*, 1979) was of such low resolution in energy (16–140 eV) and momentum ($1.5-2.0\ \hbar/a_0$) that no meaningful comparison with theory could be made; however, these experiments did confirm the feasibility of the technique. The first quantitative results on solid films were obtained by Ritter and co-workers (Gao *et al.*, 1988, 1989) who measured the spectral momentum density for carbon in graphite (parallel and perpendicular to the crystal c axis) and in amorphous carbon. These measurements were carried out with an incident-electron energy of 25 keV in order to reduce multiple-scattering effects, and employed Wien filter analyzers to obtain adequate energy and angle resolution at this high incident energy. In the intervening period other groups have undertaken the design of apparatus to study solids. It is evident that extraordinary measures must be taken to assure long-term mechanical and electronic stability, and to create and maintain cleanliness of the sample. The most recent results suggest that in the near future it will be possible to obtain binding energy spectra and perhaps also momentum density profiles for solids with nearly the same precision and resolution as currently possible with gaseous samples (Lower *et al.*, 1991).

Experiments on solids offer the possibility of measuring the momentum density profile in a direction relative to the orientation of an atom or molecule; however, this is not ordinarily possible in the gas phase where only a spherically averaged momentum density can be obtained owing to the rotational motion of the target. It is not feasible to orient a collection of atoms or molecules, but it is possible to select from all the atoms or molecules in a sample those which possess a particular orientation. Zheng *et al.* (1990) have recently demonstrated this possibility by measuring the momentum density for excited sodium atoms in aligned states prepared by optical pumping with polarized laser light.

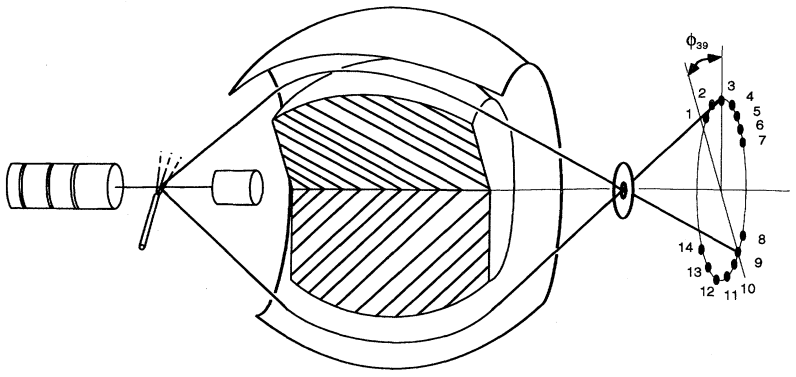

FIG. 8. Symmetric-noncoplanar $(e,2e)$ spectrometer based on a single spherical electrostatic analyzer. Only those scattered and ejected electrons of the same energy are transmitted by the analyzer to the detector plane where 14 separate channel-electron-multiplier (CEM) detectors are located. For the two electron trajectories shown on the diagram, the relative out-of-plane angle is ϕ_{59}.

V. INTERPRETATION OF (e,2e) DATA IN TERMS OF ELECTRONIC STRUCTURE

A. Atomic and molecular properties related to the (e,2e) cross section

In actual practice, $(e,2e)$ spectroscopy for the determination of electron momentum densities is always carried out in a regime in which the incident- and ejected-electron energies and the momentum transfer are sufficiently large that the process is accurately described by the plane-wave impulse approximation. As described above, this results in the expression for the cross section being separated into terms each of which depend exclusively either upon the scattering dynamics or on the electronic structure of the target. Generalizing Eq. (3.16) to the case of a many-electron atom or molecule, this expression takes the form

$$d^3\sigma_{(e,2e)}/d\Omega_a d\Omega_b dE_b = \frac{4m^2e^4}{\hbar^4K^4}(k_a k_b/k_0)|\langle \Phi_{i\alpha}|e^{i\mathbf{q}\cdot\mathbf{r}_i/\hbar}|\Psi\rangle|^2 \quad (5.1)$$

for the ejection of a target electron with coordinate $\mathbf{r}_i$ in an atom or molecule with total electronic wave function Ψ to create an ion with wave function $\Phi_{i\alpha}$ (where the first index identifies the hole left by the knocked-out electron and the second identifies the state of the ion). For the case of molecules it is assumed that the nuclei are stationary at their equilibrium positions. In the usual symmetric noncoplanar geometry, the factors in front of the absolute value sign are constant so that the $(e,2e)$ cross section is simply proportional to the last term on the right, which is equivalent to the square of the Fourier transform of the ion-neutral overlap. This expression is greatly simplified if correlation effects are not important for the target electron, as is frequently the case for a closed-shell molecular target. The target electron can then be described by a single-electron wave function ψ_i (i.e., an orbital) representable by a single Hartree-Fock determinant. Then, if electron correlation in the open-shell ion is accounted for by the use of a CI wave function represented by a linear combination of Hartree-Fock orbitals derived from the same basis set as used for the neutral, the cross section becomes

$$\sigma_{(e,2e)} = \sigma_{(e,e)}(k_a k_b/k_0)|\langle \Phi_{i\alpha}|\Psi_{-i}\rangle|^2|\langle e^{i\mathbf{q}\cdot\mathbf{r}_i/\hbar}|\Psi_i|^2 , \quad (5.2)$$

where $\Psi_{-i}=\Psi/\psi_i$. This is the *target Hartree-Fock approximation* (THFA), which forms the basis of most interpretations of $(e,2e)$ data. The term $|\langle \Phi_{i\alpha}|\Psi_{-i}\rangle|^2$ is the spectroscopic factor, which gives the probability of producing the α state of the ion upon ejection of the ith electron from the neutral target. The last term on the right, $|\langle e^{i\mathbf{q}\cdot\mathbf{r}_i/\hbar}|\psi_i\rangle|^2$, the square modulus of the Fourier transform of the single-electron wave function, is the momentum density of the target electron, $\rho(\mathbf{q}_i)$. The most rudimentary interpretation of $(e,2e)$ data adopts the frozen core approximation, equivalent to taking $\Phi_{i\alpha}$ identical to Ψ_{-i}. The spectroscopic factor is then unity and the $(e,2e)$ cross section is directly proportional to the target-electron momentum density.

A useful interpretation of measured momentum densities relies upon the relations between momentum-space and position-space descriptions of atomic and molecular electronic structure. These are described in Fig. 9 by a diagram originally constructed by Weyrich *et al.* (1979). Here we see that the position-space and momentum-space wave functions are the Fourier transform (FT) of one another. The square modulus ($|\ |^2$) of each wave function gives the density distribution in each spatial representation. Furthermore, Fourier transformation of each density function enables a transformation to the complimentary coordinate space. The Fourier transform of the momentum density yields a function in position space, $B(\mathbf{r})$, which is the autocorrelation function (AC) of the position-space wave function:

$$B(\mathbf{r})=\int \Psi^*(\mathbf{r}+\mathbf{s})\Psi(\mathbf{r})d\mathbf{s} . \quad (5.3)$$

The analogous function in momentum space, $F(\mathbf{q})$, is the familiar x-ray form factor. The directional arrows are important features of the Weyrich diagram, indicating, for example, the impossibility of obtaining uniquely the momentum-space wave function from the momentum density because of the loss of phase information in the square modulus.

The Weyrich diagram can be interpreted in two ways. In the total-electron description, $\mathbf{r}$ implies $\mathbf{r}_1\mathbf{r}_2\cdots\mathbf{r}_n$, and $\mathbf{q}$ implies $\mathbf{q}_1\mathbf{q}_2\cdots\mathbf{q}_n$. Alternatively, the diagram applies to a single-electron description ($\mathbf{r}$ implies $\mathbf{r}_i$, $\mathbf{q}$ implies $\mathbf{q}_i$). It is worth noting that for the latter case, the $(e,2e)$ experiment provides the only means to observe directly one of the functions described by the diagram.

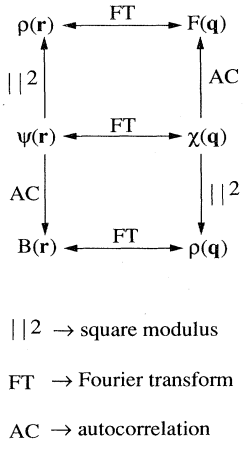

FIG. 9. Diagram showing the relation of the position-space wave function, electron density, and autocorrelation function to the corresponding functions in momentum space (Weyrich *et al.*, 1979).

With respect to total electron properties, Compton scattering and x-ray diffraction data are related to $\rho(\mathbf{q})$ and $F(\mathbf{q})$, and hence to the total-electron wave function. A further important distinction between $(e,2e)$ and Compton scattering arises when sampling an isotropic substance or unoriented molecules in the gas phase. In this case the $(e,2e)$ signal intensity depends upon the *spherically averaged momentum density* $\rho(q)$, defined by

$$\rho(q)=\int_0^{2\pi}\int_{-1}^{1}\rho(\mathbf{q})d(\cos\theta)d\phi\ , \tag{5.4}$$

whereas the Compton signal is a measure of the *radial probability distribution function,* $I(q)=\rho(q)q^2$. The probability distribution function is insensitive to the momentum-space wave function for small values of momentum owing to the small volume of phase space available for values of momentum near the momentum-space origin. Physical phenomena such as polarization and chemical phenomena such as bond formation change primarily the behavior of electrons at low momentum. As a consequence, the $(e,2e)$ technique is probably more appropriate for investigating the connection between such phenomena and the electronic wave function in spite of the fact that Compton data is generally of higher precision than $(e,2e)$ data.

B. Interpretation of $(e,2e)$ data

The interpretation of $(e,2e)$ data can proceed by one of three routes:

(1) Models can be developed that relate physical and chemical properties of materials to a momentum-space description of electronic structure. These might take the form of momentum-space orbitals and employ the momentum-space analogs of interpretive schemes such as the Woodward-Hoffman rules.

(2) Familiar position-space models can be retained and an attempt made to understand their implications for observations made in momentum space.

(3) The momentum-space data can be transformed to position space in which familiar models can be more easily applied.

The first possibility is not very promising because of the general reluctance of most physicists and essentially all chemists to think in momentum coordinates, as well as the nearly insurmountable difficulties involved in solving the integral electronic equation of motion in momentum coordinates (the momentum-space Schrödinger equation). An advantage of the momentum-space representation is that the wave function and the momentum density have relatively large amplitudes at low momentum. Thus they are sensitive in regions most obviously related to physical and chemical phenomena. On the other hand, the nuclei do not appear as points in the electron momentum space. Thus the familiar atomic center or molecular backbone is missing.

The second route largely involves an attempt to understand the effect of the Fourier transformation on the position-space wave function. This is the approach that has received most attention.

The third possibility requires an understanding of the relation between $B(\mathbf{r})$ and $\rho(\mathbf{r})$, since the familiar models used by chemists and physicists relate atomic and molecular properties to the electron-density distribution.

C. The Fourier transform of the wave function

1. Atomic orbitals

Almost all $(e,2e)$ experiments have been performed on unoriented atoms or molecules in the gas phase. Interpretation based upon the position-space orbital model of electronic structure then requires a comparison of the data with the spherical average of the square modulus of the Fourier transform of the single-electron wave function. With this approach it is most important to understand the effect of the Fourier transformation on the position-space wave function and, in particular, the spatial inversion associated with this operation. It is the nature of the Fourier transform that the amplitude at every point in r space contributes to that at each point in q space; however, the amplitude of the r-space wave function for large values of $\mathbf{r}$ is primarily responsible for the momentum density at small values of momentum, and vice versa. This also follows from the uncertainty principle. As a consequence, the momentum density near the origin in q space is always relatively large since a very large volume of position space is compressed into a very small volume of momentum space. This effect makes the momentum density especially sensitive to physical and chemical phenomena, which are governed by the behavior of the electron far from the nucleus where its motion is described by the large-r "tail" of the wave function.

Two other properties of the Fourier transform are useful in the interpretation of the momentum density in terms of the position-space orbital model. The Fourier transform of a narrow function yields a broad function, and vice versa. Thus the distribution of momentum density is broad for a localized orbital, and, conversely, a diffuse orbital yields a narrow momentum-density function. A second important property is that the nodal character of a function is preserved by a Fourier transform. A consequence is the distinctive difference in appearance between an atomic s function and a p function. An atomic p orbital has a nodal plane through the origin in both position space and momentum space and must thus yield a spherically averaged momentum density of zero for $q=0$. On the other hand, the momentum density for an atomic s orbital is a maximum at $q=0$. This is illustrated in Fig. 10 for the case of hydrogenic $2s$ and $3s$, and $2p$ and $3p$ orbitals. The figure also illustrates the effect of localization in r space. It can be seen, for example, that the $3p$ momentum-density function is more nar-

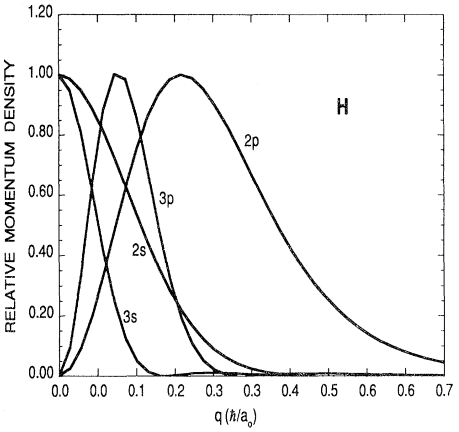

FIG. 10. Momentum densities for the hydrogen atom.

row than the $2p$, in accord with the $3p$ orbital being more diffuse than the $2p$.

2. Molecular orbitals

It is difficult to derive a wave function for a molecule from a momentum-space formulation of the problem. With the single exception of H_2^+ (McWeeny, 1949), momentum-space wave functions and momentum densities are always calculated by a Fourier transformation of a solution derived in position space. As a further practical matter, the derivation of appropriate wave functions for all but the simplest molecules is based upon the linear combination of atomic orbitals, or LCAO, model in which the molecular wave function is approximated by a sum of terms each of which is an approximation of an atomic wave function centered on an atom in the molecule. The selection of atomic orbitals included in the LCAO is based upon the symmetry of the molecule, physical intuition, and the computational power available; however, the essential features of the momentum density predicted by transforming an LCAO orbital can be understood by carrying out the process on the simplest possible wave functions as illustrated by Coulson and Duncanson in an elegant series of papers in 1940 and 1941 (Coulson, 1941a, 1941b; Coulson and Duncanson, 1941a, 1941b; Duncanson, 1941; Duncanson and Coulson, 1941).

The most elementary LCAO wave function for a one-electron homonuclear diatomic molecule has the form

$$\psi_{\pm}(\mathbf{r})=\frac{1}{\sqrt{2(1\pm S)}}[\psi_{a0}(\mathbf{r})\pm\psi_{a0}(\mathbf{r}-\mathbf{R})]\ , \tag{5.5}$$

where ψ_{a0} is an atomic wave function; $\mathbf{R}$ is the internuclear vector, and the coordinate system is located on one of the nuclear centers; and S is the overlap integral between $\psi_{a0}(\mathbf{r})$ and $\psi_{a0}(\mathbf{r}-\mathbf{R})$. For purposes of illustration, we consider the case in which a plus sign gives the bonding molecular wave function while a minus sign gives the antibonding wave function for which there is a nodal plane between the two atoms. Taking the Fourier transform and squaring the result gives the momentum density

$$\rho(\mathbf{q})=|\xi_{\pm}(\mathbf{q})|^2=|\xi_{a0}(\mathbf{q})|^2\frac{1\pm\cos\frac{\mathbf{q}\cdot\mathbf{R}}{\hbar}}{1\pm S}\ . \tag{5.6}$$

The first term of the product on the right is the momentum density of the atomic wave function. All information about the bond between the atoms is contained in the second term. Because of the cosinusoidal variation of this term it is called the *interference term* or *diffraction factor*. For the bonding combination, the interference term vanishes for $\mathbf{q}\cdot\mathbf{R}/\hbar=(2n+1)\pi$, and the momentum density along the bond direction oscillates with a period of $2\pi/R$. Furthermore, the interference term is a maximum for $\mathbf{q}$ perpendicular to $\mathbf{R}$, and thus for a given magnitude of $\mathbf{q}$ there is a greater probability that the momentum is oriented perpendicular to the bond than that it is parallel. The opposite is true for the antibonding combination. Thus, when electron density is concentrated along a bond, the momentum density is concentrated in the direction perpendicular to the bond, and vice versa. The so-called *bond oscillation* associated with the interference term is rarely observed in the spherically averaged single-electron momentum density because the atomic term damps the interference term nearly to zero as $q/\hbar=2\pi/R$ is approached. Experimental verification of this has been done by Bharathi *et al.* (1991).

Many properties of the single-electron molecular momentum density can be illustrated with the minimum-basis-set LCAO wave function given above. Atomic s-orbital basis functions give two molecular orbitals, σ_g and σ_u, respectively bonding and antibonding. The σ_g is totally symmetric and, like the atomic s orbital, gives an s-type spherically averaged momentum density [Fig. 11(a)]. The σ_u has a nodal plane perpendicular to and bisecting the internuclear axis, which, being also a plane of symmetry, appears in momentum space as a nodal plane through the origin. The σ_u momentum density thus is similar to the atomic p-type density function [Fig. 11(b)]. In fact, since only the σ_g is totally symmetric, all other molecular orbitals of a homonuclear give p-type momentum-density functions.

The linear combination of atomic p orbitals may give σ or π molecular orbitals depending on the orientation of the p function (that is, projection of the angular momentum vector) with respect to the internuclear axis (conventionally taken as the z direction). The π orbital wave functions may be defined by

$$\psi_{\pi_{x,y}}(\mathbf{r})=N_{\pm}(\psi_{p_{x,y}}(\mathbf{r})\pm\psi_{p_{x,y}}(\mathbf{r}-\mathbf{R}))\ . \tag{5.7}$$

The bonding combination (π_u) and antibonding combination (π_g) both have a planar nodal surface coinciding with a symmetry plane containing the internuclear axis and thus yield p-type momentum-density functions [Figs.

11(c) and 11(d)]. The π_g has an additional nodal plane perpendicular to and bisecting the internuclear axis, resulting in two nodal planes through the origin in q space. This has the effect of reducing the volume of phase space available to momentum density at small q. The result [Fig. 11(d)] is a displacement of the maximum in the momentum density function to higher q relative to the corresponding, bonding π orbital. This effect for antibonding interactions may also be understood from a consideration of the momentum operator. The momentum depends upon the gradient of the position-space wave function. Rapid variation of the antibonding wave function in the internuclear region yields an increased probability of high momentum components compared to the case for the bonding wave function. Note also the difference in the width of the momentum-density function between the bonding and antibonding orbitals. The antibonding wave function in r space is localized at the nuclear centers, whereas the bonding function is more diffuse, extending into the region of the bond. As a consequence, the bonding momentum density is localized and the antibonding density relatively more diffuse.

The inclusion of p_z atomic orbitals in the representation of σ molecular orbitals provides one last illustrative example:

$$\psi_{p\sigma}(\mathbf{r})=N_{\mp}[(a\psi_{p_z}(\mathbf{r})+b\psi_s(\mathbf{r})) \mp(a\psi_{p_z}(\mathbf{r}-\mathbf{R})-b\psi_s(\mathbf{r}-\mathbf{R}))] , \tag{5.8}$$

where the coefficients a and b determine the relative p_z and s contributions. The corresponding momentum-density function is

$$\rho(\mathbf{q})=|\xi_{p\sigma}(\mathbf{q})|^2 =2N_{\mp}^2\left[a^2|\xi_{p_z}(\mathbf{q})|^2\left[1\pm\cos\frac{\mathbf{q}\cdot\mathbf{R}}{\hbar}\right] +b^2|\xi_s(\mathbf{q})|^2\left[1\pm\cos\frac{\mathbf{q}\cdot\mathbf{R}}{\hbar}\right]\right] . \tag{5.9}$$

The bonding σ_g has momentum density proportional to b^2 at $\mathbf{q}=0$ [Fig. 11(e)], whereas the antibonding σ_u with a planar nodal surface between the atoms in position space, and thus a nodal plane through the momentum-space origin, yields a p-type spherically averaged momentum-density function [Fig. 11(f)]. In addition to the nodal plane associated with the antibonding combination, both σ_g and σ_u have a nodal surface associated with the nodal surface in the p basis functions. This nodal surface in r space is ellipsoidal and yields an ellipsoidal nodal surface with its major axis in the perpendicular direction in momentum space.

Classification of features in the momentum density becomes less clear as one proceeds from homonuclear diatomics to heteronuclear diatomics to polyatomics. For example, the nodal surface associated with antibonding interactions in a heteronuclear molecule is not planar. As a result the corresponding nodal surface in momentum space does not pass through the origin, and thus the antibonding momentum density will have both s character (with nonzero amplitude at the origin) and p character (with a local maximum at an intermediate value of q). Nevertheless, some useful observations can be made on the basis of group theory.

Molecular orbitals are classified according to how they transform under the operations of the group to which the molecule belongs. An orbital is given the name of the representation that transforms in the same manner as the orbital (hence σ_g, σ_u, and so on). The symmetry elements of the orbital are preserved under Fourier transformation. In addition, the requirement of zero net momentum in the rest frame of the molecule introduces a center of inversion to the momentum-space symmetry group (unless one already existed in position space). Thus, for example, the orbitals of a molecule such as H_2O, which belong to the C_{2v} group in r space, belong to D_{2h} in q space. In momentum space, all orbitals except those that transform as the totally symmetric representation of the group will have a node at the origin. In H_2O, the a_1 orbitals may have nonzero (spherically averaged) momen-

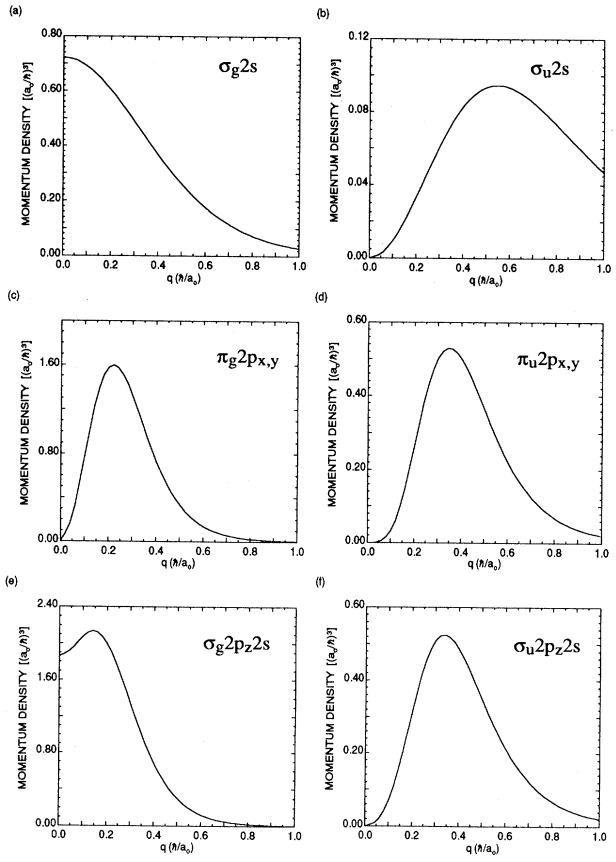

FIG. 11. Molecular momentum densities derived from minimum-basis-set LCAO wave functions for a homonuclear diatomic (see text for details).

tum density at $q=0$; all others (a_2, b_1, and b_2) will have p-type spherically averaged momentum-density functions. Qualitative observation of the shape of the momentum density measured by $(e,2e)$ along with a consideration of the ionization energy often permit an unambiguous assignment of the orbital in which an electron resides—an advantage over other spectroscopies.

D. Measurements on acetylene and water

The frozen-core approximation is obviously unsatisfactory when satellite peaks appear in the binding energy spectrum. These are peaks corresponding to ionization energies higher than would be required to remove an electron to leave an ion in a single-hole state (represented by $\Phi_{i\alpha}$). To a first approximation, the satellite excitations can be attributed to two-electron processes resulting from electron-correlation effects in the ion. Such effects can be accounted for through the use of an appropriate multiple-configuration, or configuration interaction (CI), wave function to represent the ion to give the cross-section expression in Eq. (5.2) (the target Hartree-Fock approximation). The spectroscopic factors can then be compared with satellite intensities while the shape of the cross section corresponds to the momentum density for the target-electron orbital in the neutral.

Investigations of satellite structure in $(e,2e)$ spectra have been valuable in assigning the origin of the corresponding ionization process and in evaluating quantum-mechanical calculations that attempt to describe electron correlation. The ionization spectrum of acetylene, C_2H_2, has probably received the greatest attention, with many UV and x-ray photoionization studies, as well as at least four $(e,2e)$ studies (Weigold *et al.*, 1976; Dixon *et al.*, 1977; Coplan *et al.*, 1978, Weigold *et al.*, 1991, Duffy *et al.*, 1992), reported over the past 25 years. Although the resolution in the $(e,2e)$ binding energy spectrum shown in Fig. 12 does not equal that of most photoionization spectra, extensive satellite intensity above 25 eV is evident in addition to peaks associated with direct single-electron ejection from the valence orbitals, $1\pi_u$, $3\sigma_g$, $2\sigma_u$, and $2\sigma_g$. The origins of the satellite intensity, that is, the parent hole states, cannot be determined unambiguously from the photoelectron spectra, although various theoretical calculations have attributed intensity in varying degrees to ionizations involving the $2\sigma_u$ and $2\sigma_g$ electrons. The target Hartree-Fock approximation (THFA) description of the $(e,2e)$ cross section seems to serve well here, at least qualitatively, as shown, for example, in the inset in Fig. 12 for the satellite intensity near 28 eV. The $(e,2e)$ cross section measured for the 28 eV energy loss has the characteristic s-type shape thus confirming the $2\sigma_g$ as the origin of the satellite electron in this region. Measurement of the shape and relative amplitude of the $(e,2e)$ cross sections for the single-hole (parent) ionizations, as well as the multiple-hole (satellite) ionizations, provides a stringent test of theoretical wave functions, since both energies and spectroscopic factors

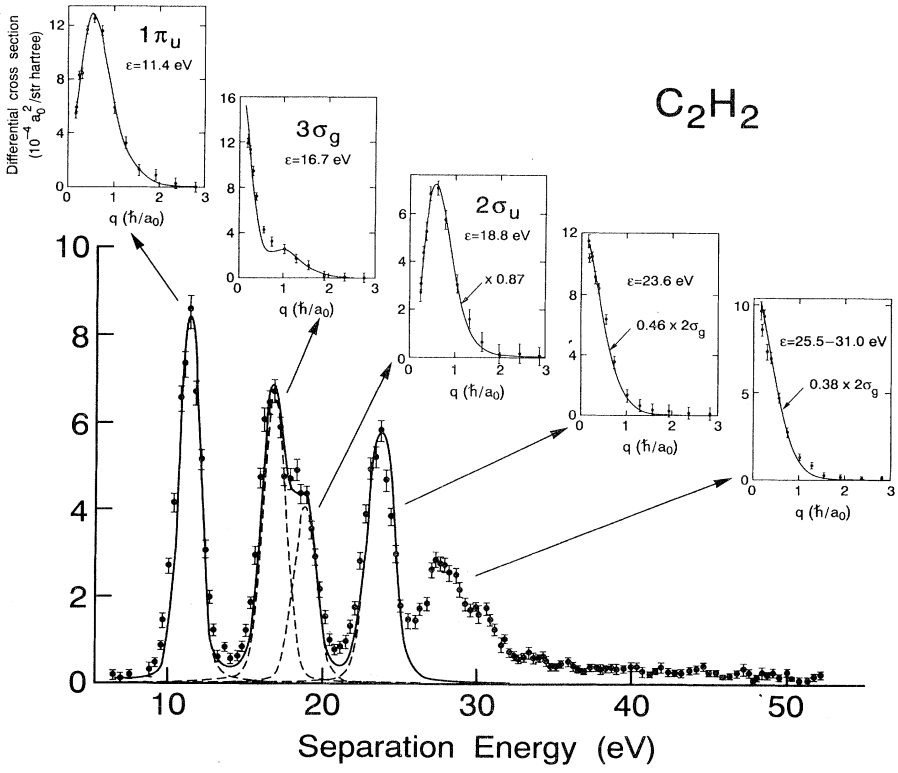

FIG. 12. Binding energy spectrum from acetylene with insets showing the $(e,2e)$ cross section at selected energies. Peaks at 11.4, 16.7, 18.8, and 23.6 eV correspond to single-hole states derived from ionization of the valence electrons. 87% of the expected density is found at the energy of the $2\sigma_u$ primary-hole state and only 46% for the $2\sigma_g$ primary hole. The shape of the cross section in the 25–31 eV region is similar to that for the $2\sigma_g$, implying that satellites in this region (associated with simultaneous ionization and excitation) are derived from ionization of the $2\sigma_g$ electron. The missing $2\sigma_u$ amplitude is believed to be distributed throughout the satellite region (Weigold *et al.*, 1991).

(in the case of the THFA) or overlap integrals (when initial-state correlation effects are considered) must be calculated. In the case of acetylene, large-basis-set single-configuration wave functions, as well as CI wave functions, have been used to accurately describe the shape of the momentum-density functions of the valence orbitals. Predictions of the amplitude of the $(e,2e)$ cross section using CI wave functions have not been very satisfactory; however, a recent Green's-function calculation (Weigold *et al.*, 1991) gives excellent agreement with experiment.

Dramatic evidence of the effect of electron correlation upon the momentum density is provided by the example of the outermost valence orbital of H_2O shown in Fig. 13 (Bawagan *et al.*, 1987). To model the experimentally observed momentum density, THFA calculations using an extreme range of theoretical wave functions have been employed. The trend usually observed with expansion and optimization of the wave functions are evident in the figure. The minimum-basis-set function (MBS) fails to account for a significant part of the density at low momentum. A near-Hartree-Fock calculation (NHF) yields an improvement but still falls short in the low-momentum region. This can be attributed to the fact that variational optimization, which in this case gives an accurate energy, is insensitive to the diffuse (i.e., large-r) parts of the wave function, which are important in describing chemical phenomena. A calculation of the momentum-density function using a greatly extended basis set, the 109-GTO incorporating Gaussian-type functions of s, p, d, and f symmetry, and, ultimately, a calculation of the ion-neutral overlap [Eq. (5.2)] using CI wave functions based upon the 109-GTO basis set for both initial and final states results in even closer agreement between theory and experiment. The remaining discrepancy in the low-momentum region has been attributed to the finite resolution of the experiment (Bawagan and Brion, 1990).

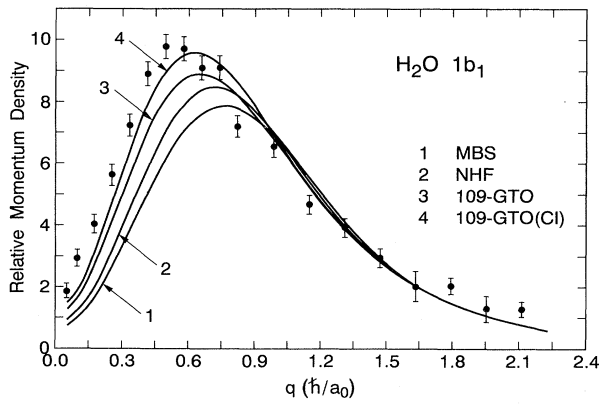

FIG. 13. $(e,2e)$ momentum density for the $1b_1$ orbital of water along with calculations in the target Hartree-Fock approximation based upon minimum-basis-set (MBS), near-Hartree-Fock (NHF), and greatly extended basis set (109-GTO) wave functions, and a calculation of the Fourier transform of the ion-neutral overlap using CI wave functions based upon the 109-GTO basis set (109-GTO CI) (Bawagan *et al.*, 1987).

E. Fourier transform of the momentum density

The Fourier transform of the momentum density, $B(\mathbf{r})$, has been examined by a number of workers (Benesch *et al.*, 1971; Weyrich *et al.*, 1979; Thakkar *et al.*, 1981), especially for the case of Compton profiles, since the time of Coulson's original work (Coulson, 1941a, 1941b; Coulson and Duncanson, 1941a, 1941b; Duncanson, 1941; Duncanson and Coulson, 1941). The $B(\mathbf{r})$ function provides an alternative way of interpreting momentum densities. This function, equivalent to the autocorrelation function of the spatial wave function [Eq. (5.3)], is given by

$$B(\mathbf{r})=\frac{1}{(2\pi)^{3/2}}\int \rho(\mathbf{q})\exp(i\mathbf{q}\cdot\mathbf{r}/\hbar)d\mathbf{q}\ , \tag{5.10}$$

where, as above, $\rho(\mathbf{q})=|\xi(\mathbf{q})|^2$, and

$$\xi(\mathbf{q})=\frac{1}{(2\pi)^{3/2}}\int \psi(\mathbf{r})\exp(i\mathbf{q}\cdot\mathbf{r}/\hbar)d\mathbf{r}\ .$$

For $r=0$, $B(\mathbf{r})$ is the normalization integral with a value of unity. $B(\mathbf{r})$ functions have their maximum values at $\mathbf{r}=0$, and are generally small at $\mathbf{r}$ values beyond 1 a.u.

The usefulness of the $B(\mathbf{r})$ function compared with the momentum density can be illustrated with the simple example of the one-electron homonuclear diatomic molecule treated in the previous section. The $B(\mathbf{r})$ function is obtained by taking the Fourier transform of Eq. (5.6). The result is

$$B(\mathbf{r})=\frac{B_{a0}(\mathbf{r})\pm\frac{1}{2}[B_{a0}(\mathbf{r}+\mathbf{R})+B_{a0}(\mathbf{r}-\mathbf{R})]}{(1\pm S)}\ , \tag{5.11}$$

where $B_{a0}(\mathbf{r})$ is the autocorrelation function of $\psi_{a0}(\mathbf{r})$. The positive sign is for the bonding wave function and the negative sign is for the antibonding wave function. As discussed in the preceding section, the interference term or diffraction factor is almost never seen in the momentum density because of its modulation by the rapidly decreasing atomic momentum-density term. On the other hand, the modulation in the $B(\mathbf{r})$ function for the antibonding wave function is observable. At $\mathbf{r}=\mathbf{R}$ both $B_{a0}(\mathbf{r})$ and $B_{a0}(\mathbf{r}+\mathbf{R})$ are small, while $B_{a0}(\mathbf{r}-\mathbf{R})$ has its maximum value. The result is an extremum in the function in the region of the bond length. This simple example can be extended to more complex wave functions and polyatomic molecules. The interpretation of single-electron momentum densities through the transformation back to r space has been pursued primarily by Tossell *et al.* (1981). The key to this approach was the realization that the Fourier transform of the experimentally accessible, spherically averaged, single-electron momentum density yields $B(r)$, the spherical average of the autocorrelation of the position-space wave function (Weyrich

et al., 1979; Tossell *et al.*, 1981):

$$B(r)=\int_0^{2\pi}\int_{-1}^{1} B(\mathbf{r})r^2 d(\cos\theta)d\phi$$
$$=4\pi\int_0^{\infty}\left[\frac{\sin(qr/\hbar)}{qr/\hbar}\right]\rho(q)q^2dq\ . \qquad (5.12)$$

As might be expected, this one-dimensional autocorrelation function is rather featureless, starting with a value of identically 1 at $r=0$, and typically falling to 0.1 within a distance of the order of a bond length; however, successful comparisons of $B(r)$ functions have been made by examining the difference between two $B(r)$ functions, $\Delta B(r)$. An assessment of a theoretical wave function can be made by looking at the difference between $B(r)$ derived from experimental data and $B(r)$ calculated from theory. Details of the electron density associated with chemical bonding have been delineated in comparisons of $B(r)$ for analogous orbitals in structurally related molecules. For example, the role of the nitrogen $2p$ "lone pair" in amines has been investigated by comparing $B(r)$ for this orbital in a substituted amine and to that for the lone pair in ammonia (Tossell *et al.*, 1984). Some caution must be observed in the calculation of a difference function from experimental data; $\Delta B(r)$ seldom exceeds a value of 0.1, so relatively precise and accurate data are required.

An example of the $\Delta B(r)$ approach is given in a recent $(e,2e)$ study of bonding in a Lewis acid-base complex (McMillan *et al.*, 1990). In this case the Lewis acid is boron trifluoride BF_3, and the Lewis base, the electron donor, is trimethyl amine $(CH_3)_3N$. The donor-acceptor complex, $(CH_3)_3N{:}BF_3$, is bound by the donation of the $N2p$ lone-pair electrons of the amine to the incompletely filled valence shell of boron. The way in which the lone-pair electrons of the amine were rearranged upon the formation of the bond was examined through momentum-density measurements of the highest occupied molecular orbital of the amine, the "lone pair" identified as $6a_1$, and the analogous orbital in the complex, identified as $11a_1$. These measurements are shown in Fig. 14. Both orbitals transform as the totally symmetric representation (a_1) in the group to which the molecules belong, and there is no node at the momentum-space origin. It is possible to associate features of the measured momentum densities with the major atomic-orbital contributions to the wave functions. In the momentum density for both molecules the amplitude near the origin comes from the methyl hydrogen $1s$ and the $N2s$ atomic orbitals. For the $6a_1$ orbital of the amine, the amplitude near $q=1.0\ \hbar/a_0$ is due to the $N2p$. For the analogous $11a_1$ orbital in $(CH_3)_3N{:}BF_3$, the local maximum near $0.5\ \hbar/a_0$ comes from the $N2p$ as in the amine. The more complex shape of the momentum density for the $11a_1$ orbital in $(CH_3)_3N{:}BF_3$ is a reflection of the complex nodal structure of this orbital. The nature of the interaction of the important atomic contributions can be understood from the $\Delta B(r)$ plot in Fig. 15, which compares the acid-base

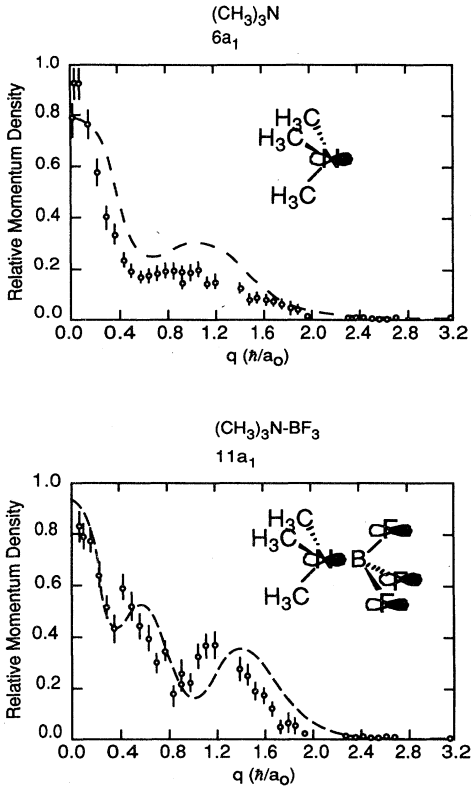

FIG. 14. $(e,2e)$ data for the highest-occupied molecular orbital of trimethyl amine, the $6a_1$ "lone pair," and for the analogous orbital in the trimethyl amine-boron trifluoride complex. The dashed line gives the momentum density calculated from $3-21G^+$ wave functions (McMillan *et al.*, 1990).

complex to the amine. A positive extremum in $\Delta B(r)$ corresponds to a value of r equal to the distance between the region of the $N2p$ lobe between the boron and nitrogen and the $F2p$ lobe of the same sign. The value of r at which the negative extremum in $\Delta B(r)$ occurs corresponds to the distance between that same $N2p$ lobe and

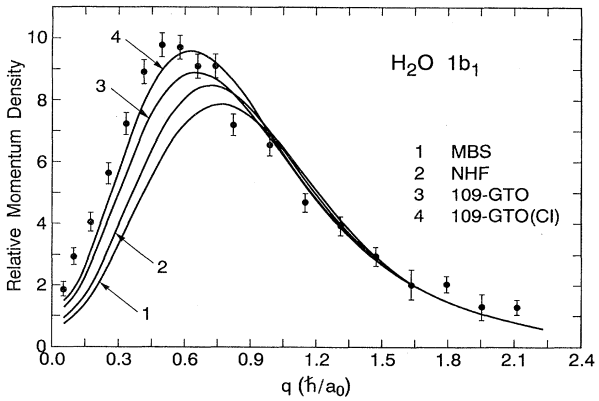

FIG. 15. Autocorrelation difference function, $\Delta B(r)=B(r)_{\text{complex}}-B(r)_{\text{amine}}$, derived from the data in Fig. 14 (McMillan *et al.*, 1990).

the oppositely signed $F2p$ lobe. Since the negative extremum occurs at a smaller distance than the positive extremum, an antibonding $N2p-F2p$ interaction is indicated, suggesting a weakening of the boron-fluorine bond in the BF_3 moiety upon formation of the complex.

F. Current state of electronic structure determination from (e,2e) experiments

Experiments carried out nearly two decades ago demonstrated the use of the $(e,2e)$ reaction for measuring single-electron momentum densities for the outer electrons in atoms and spherically averaged, single-electron momentum densities for valence electrons in molecules. Subsequent work defined the geometry and energy range where the results of $(e,2e)$ experiments could most conveniently and reliably be interpreted in terms of the target-electron momentum density. In practice this amounted to experimental and theoretical confirmation of the regime in which the accuracy of the plane-wave impulse approximation was consistent with the precision of the experiments. During the 1970s the sensitivity of the technique was developed to the point where experimentally measured momentum densities could be used to distinguish between theoretical predictions based upon different approximations to the Hartree-Fock wave function. During the past decade, $(e,2e)$ experiments on small molecules have proven to be sufficiently accurate to distinguish between very-large-basis-set, single-determinant methods and multiconfiguration approximations. The $(e,2e)$ technique has been applied to large polyatomic molecules and even to models of reacting systems. A bibliography compiled by Leung (1991) cites measurements of momentum densities for the valence electrons in at least 48 polyatomic molecules (triatomics up to 40-atom species). Some progress has been made in qualitatively analyzing momentum densities and their Fourier transforms in terms of the familiar models of electronic structure employed by chemists and physicists. In favorable cases it has been possible to attribute features in the single-electron, spherically averaged molecular momentum density, as well as density differences between related molecules, to well-defined chemical effects.

Two decades of work on the experimental determination of atomic and molecular electron momentum densities have documented the value of the $(e,2e)$ technique as well as some of its shortcomings, the most obvious being practical limitations to precision and resolution and the fact that only the spherically averaged momentum density can be obtained in experiments on molecules in the gas phase. In state-of-the-art $(e,2e)$ apparatus designed for the investigation of momentum densities, using data collection times of the order of one day, cross sections are measured with a precision of 3–5 % of the maximum value. The best attainable angular and energy resolution in these experiments corresponds to momentum resolution of $0.07-0.15\ \hbar/a_0$. In the region of target momenta above about $0.5\ \hbar/a_0$, this is adequate for the comparison of experimental results and the predictions of high-level calculations. In the low-momentum region most sensitive to chemical phenomena, the finite resolution can lead to differences between experiment and theory of a factor of 2 or more, especially for p-type momentum densities where the cross section increases rapidly as the momentum increases from zero. Finite resolution in the experimental apparatus also produces a distortion of the momentum scale for low values of momentum. This is a result of the fact that the experiment determines only the absolute value of the momentum corresponding to a particular set of scattering angles (see Table II). The resolution function, which might reasonably be considered to have a symmetric Gaussian shape, is folded back on itself at the zero of momentum. This yields a skewed resolution function at low momentum so that with finite resolution the nominal momentum value being sampled is different from the mean. These effects have been modeled in Monte Carlo simulations of the experiments in an effort to account for discrepancies between experimental observations and theoretical calculations (Bawagan and Brion, 1990).

A great deal of the information contained in the single-electron momentum-density function is obscured by the spherical averaging associated with a measurement on a freely rotating molecule in the gas phase. There have been proposals (Camilloni *et al.*, 1979) and even experiments to measure directed momentum densities. Compton scattering on crystals gives directed momentum densities averaged over all electrons. Zheng *et al.* (1990) have performed $(e,2e)$ experiments on laser-excited, oriented atoms; however, this approach will not be applicable to molecules because the broad rotational energy distribution in a molecular sample is incompatible with the narrow-band nature of laser light. The early $(e,2e)$ measurements on carbon films (Amaldi *et al.*, 1969; Camilloni *et al.*, 1972; Ritter, Dennison, and Jones, 1984) and the recent success of Weigold *et al.* and Lower *et al.* (1991) in obtaining spectral momentum densities at high resolution in amorphous carbon suggest that measurements on oriented molecules in condensed phases may be possible in the near future; however, one cannot expect that the precision of such experiments will equal that obtained in current gas-phase experiments because of the intense background of electrons scattered from the substrate.

ACKNOWLEDGMENTS

We wish to acknowledge the help and advice of a large number of colleagues and associates. We are particularly grateful to the many workers in the field who made available reprints and preprints of their work: C. Whelan, L. Avaldi, E. Weigold, I. McCarthy, A. Lahmam-Bennani, G. Stefani, R. Camilloni, H. Ehrhardt, J. Cooper, C. E. Brion, K. T. Leung, A. L. Ritter, L. Frost, J. Briggs, A. Bawagan, F. Read, W. Nakel, J. Williams, P. Best, L. S.

Cederbaum, W. Domcke, W. von Niessen, V. Smith, Jr., and J. A. Tossell.

Support of the National Science Foundation under grants CHE-8808589, PHY-91-07337, and ATM-9222344 is gratefully acknowledged. Additional support was provided by a NATO collaborative research grant (CRG 920101) and a University of Maryland Faculty Research Award to J. H. M.

REFERENCES

Amaldi, U., A. Egidi, R. Marconero, and G. Pizzella, 1969, Rev. Sci. Instrum. **40**, 1001.
Avaldi, L., R. Camilloni, E. Fainelli, and G. Stefani, 1987a, J. Phys. B **20**, 4163.
Avaldi, L., R. Camilloni, E. Fainelli, G. Stefani, A. Franz, H. Klar, and I. E. McCarthy, 1987b, J. Phys. B **20**, 5827.
Avaldi, L., R. Camilloni, P. Letardi, G. Stefani, I. E. McCarthy, X. Zhang, H. R. J. Walters, and C. Whelan, 1992, Z. Phys. D **23**, 341.
Avaldi, L., R. Camilloni, Yu. V. Popov, and G. Stefani, 1986, Phys. Rev. A **33**, 851.
Banjavcic, M. P., T. A. Daniels, and K. T. Leung, 1991, Chem. Phys. **155**, 309.
Bawagan, A. O., and C. Brion, 1990, Chem. Phys. **144**, 167.
Bawagan, A. O., C. E. Brion, E. R. Davidson, and D. Feller, 1987, Chem. Phys. **113**, 19.
Beaty, E., 1975, Radiat. Res. **64**, 70.
Beaty, E. C., K. H. Hesselbacher, S. P. Hong, and J. H. Moore, 1977, J. Phys. B **10**, 611.
Benesch, R., S. R. Singh, and V. H. Smith, Jr., 1971, Chem. Phys. Lett. **10**, 151.
Best, P. E., and H. Zhu, 1985, Rev. Sci. Instrum. **56**, 389.
Bethe, H., 1930, Ann. Phys. (Germany) **5**, 325.
Bethe, H., 1940, Phys. Rev. **57**, 1125.
Bharathi, S. M., A. M. Grisogono, A. Lahmam-Bennani, R. Pascual, and E. Weigold, 1991, J. Electron Spectrosc. Relat. Phenom. **53**, 271.
Bransden, B. H., J. J. Smith, and K. H. Winters, 1978, J. Phys. B **11**, 3095.
Brauner, M., J. S. Briggs, H. Klar, 1989, J. Phys. B **22**, 2265.
Brion, C. E., 1975, Radiat. Res. **64**, 37.
Byron, R. W., Jr., C. J. Joachain, 1989, Phys. Rep. **179**, 211.
Byron, R. W., Jr., C. J. Joachain, and B. Piraux, 1980, J. Phys. B **13**, L673.
Byron, R. W., Jr., C. J. Joachain, and B. Piraux, 1982, J. Phys. B **15**, L293.
Byron, R. W., Jr., C. J. Joachain, and B. Piraux, 1986, J. Phys. B **19**, 1201.
Camilloni, R., A. Giardini-Guidoni, I. E. McCarthy, and G. Stefani, 1978, Phys. Rev. A **17**, 1634.
Camilloni, R., A. Giardini-Guidoni, I. E. McCarthy, and G. Stefani, 1980, J. Phys. B, At. Mol. Opt. Phys. **13**, 397.
Camilloni, R., A. Giardini, R. Tiribelli, and G. Stefani, 1972, Phys. Rev. Lett. **29**, 618.
Camilloni, R., G. Stefani, R. Fantoni, and A. Giardini-Guidoni, 1979, J. Electron Spectrosc. Relat. Phenom. **17**, 209.
Camilloni, R., G. Stefani, R. Fantoni, R. Marconero, and A. Giardini-Guidoni, 1980, Phys. Lett. A **77**, 19.
Chamberlain, O., and E. Segré, 1952, Phys. Rev. **87**, 81.
Chant, N. S., and P. G. Roos, 1977, Phys. Rev. C **15**, 27.
Cherid, M., F. Gélébart, A. Pochat, R. J. Tweed, X. Zhang, C. T. Whelan, and H. R. J. Walters, 1992, Z. Phys. D **23**, 347.
Cook, J. P. D., I. E. McCarthy, A. T. Stelbovics, and E. Weigold, 1984, J. Phys. B **17**, 2339.
Cook, J. P. D., J. Mitroy, and E. Weigold, 1984, Phys. Rev. Lett. **52**, 1116.
Coplan, M. A., A. L. Migdall, J. H. Moore, and J. A. Tossell, 1978, J. Am. Chem. Soc. **100**, 5008.
Coulson, C. A., 1941a, Proc. Camb. Philos. Soc. **37**, 55.
Coulson, C. A., 1941b, Proc. Camb. Philos. Soc. **37**, 74.
Coulson, C. A., and W. E. Duncanson, 1941a, Proc. Camb. Philos. Soc. **37**, 100.
Coulson, C. A., and W. E. Duncanson, 1941b, Proc. Camb. Philos. Soc. **37**, 67.
Crothers, D. S. F., 1986, J. Phys. B **19**, 463.
Cvejanovic, S., and F. H. Read, 1974, J. Phys. B **14**, 1841.
Dalton, J., 1808, *A New System of Chemical Philosophy* (Bickerstaff, Manchester/London), pp. 141–143.
Daoud, A., A. Lahmam-Bennani, A. Duguet, C. Dal Cappello, and C. Tavard, 1985, J. Phys. B, At. Mol. Phys. **18**, 141.
Dixon, A. J., I. E. McCarthy, C. J. Noble, and E. Weigold, 1978, Phys. Rev. A **17**, 597.
Dixon, A. J., I. E. McCarthy, E. Weigold, and G. R. J. Williams, 1977, J. Electron Spectrosc. Relat. Phenom. **12**, 239.
Doering, J. P., and L. Goembel, 1991, J. Geophys. Res. **96**, 16025.
Duffy, P., S. A. C. Clark, C. E. Brion, M. E. Casida, D. P. Chong, E. R. Davidson, and C. Maxwell, 1992, Chem. Phys. **159**, 347.
Duguet, A., M. Cherid, A. Lahmam-Bennani, A. Franz, and H. Klar, 1987, J. Phys. B **20**, 6145.
Duncanson, W. E., 1941, Proc. Camb. Philos. Soc. **37**, 397.
Duncanson, W. E., and C. A. Coulson, 1941, Proc. Camb. Philos. Soc. **37**, 406.
Dupre, C., A. Lahmam-Bennani, A. Duguet, F. Mota-Furtado, P. F. O'Mahony, and C. Dal Cappello, 1992, J. Phys. B **25**, 259.
Ehrhardt, H., G. Knoth, and P. Schlemmer, 1985, Phys. Lett. A **110**, 92.
Ehrhardt, H., M. Fischer, and K. Jung, 1982a, Z. Phys. A **304**, 119.
Ehrhardt, H., M. Fischer, K. Jung, V. M. Byron, Jr., C. J. Joachain, and B. Piraux, 1982b, Phys. Rev. Lett. **48**, 1807.
Ehrhardt, H., K. H. Hesselbacher, K. Jung, M. Schulz, and K. Willmann, 1972a, J. Phys. B, At. Mol. Opt. Phys. **5**, 2107.
Ehrhardt, H., K. H. Hesselbacher, K. Jung, and K. Willmann, 1972b, J. Phys. B **5**, 1559.
Ehrhardt, H., K. Jung, G. Knoth, and P. Schlemmer, 1986, Z. Phys. D **1**, 3.
Ehrhardt, H., M. Schulz, T. Tekaat, and K. Willmann, 1969, Phys. Rev. Lett. **22**, 89.
Fantoni, R., A. Giardini-Guidoni, R. Tiribelli, R. Camilloni, and G. Stefani, 1980, Phys. Lett. **71**, 335.
Frost, L., P. Freienstein, and M. Wagner, 1990, J. Phys. B **23**, L715.
Furness, J. B., and I. E. McCarthy, 1973, J. Phys. B **6**, 2280.
Fuss, I., I. E. McCarthy, C. J. Noble, E. Weigold, 1978, Phys. Rev. A **17**, 604.
Gao, C., A. L. Ritter, J. R. Dennison, and N. A. W. Holtzwarth, 1988, Phys. Rev. B **327**, 3914.
Gao, C., Y. Y. Wang, A. L. Ritter, and J. R. Dennison, 1989, Phys. Rev. Lett. **62**, 945.
Gélébart, F., P. Defrance, and J. Peresse, 1990, J. Phys. B **23**, 1337.
Gélébart, F., and R. Tweed, 1990, J. Phys. B **23**, L641.

Geltman, S., 1974, J. Phys. B **7**, 1994.
Giardini-Guidoni, A., R. Camilloni, and G. Stefani, 1980, in *Coherence and Correlation in Atomic Collisions,* edited by H. Kleinpoppen and J. F. Williams (Plenum, New York), p. 13.
Giardini-Guidoni, A., R. Fantoni, R. Tiribelli, D. Vinciguerra, R. Camilloni, and G. Stefani, 1978, J. Chem. Phys. **71**, 3182.
Glassgold, A. E., and G. Ialongo, 1968, Phys. Rev. **178**, 151.
Goembel, L., 1992, Ph. D. thesis (Johns Hopkins University).
Goruganthu, R. R., M. A. Coplan, J. H. Moore, J. A. Tossell, 1988, J. Chem. Phys. **89**, 25.
Hammond, P., F. H. Read, S. Cvejanovic, and G. C. King, 1985, J. Phys. B **18**, L141.
Hamnett, A., W. Stoll, G. Branton, C. E. Brion, and M. J. Van der Wiel, 1976, J. Phys. B **9**, 945.
Hayes, P., M. A. Bennett, J. Flexman, and J. F. Williams, 1988, Rev. Sci. Instrum. **59**, 2445.
Higgins, W., 1789, *A Comparative View of the Phlogistic and Antiphlogistic Theories,* reprinted in *The Life and Work of William Higgins, Chemist, 1763-1825,* by T. S. Wheeler and J. Partington (Pergamon, New York, 1960).
Hood, S. T., A. Hamnett, and C. E. Brion, 1977, J. Electron Spectrosc. Relat. Phenom. **7**, 205.
Hood, S. T., I. E. McCarthy, P. J. O. Teubner, and E. Weigold, 1973, Phys. Rev. A **8**, 2494.
Inokuti, M., 1971, Rev. Mod. Phys. **43**, 297.
Jetzke, S., J. Zaremba, and F. H. M. Faisal, 1989, Z. Phys. D **11**, 63.
Joachain, C. J., P. Franken, A. Maquet, P. Martin, and V. Veniard, 1988, Phys. Rev. Lett. **61**, 165.
Joachain, C. J., and B. Piraux, 1986, Comments At. Mol. Phys. **17**, 261.
Jones, T. J., S. Cvejanovic, F. H. Read, and M. B. Woolf, 1990, in *Proceedings of the Sixteenth International Conference of the Physics of Electronic and Atomic Collisions,* New York, 1989, edited by A. Dalgarno, R. S. Freund, M. S. Lubell, and T. B. Lucatorto (AIP, New York), p. 223.
Jones, R., and A. L. Ritter, 1986, J. Electron Spectrosc. Relat. Phenom. **40**, 285.
Julg, A., 1980, *La Liason Chimique,* Collection Encyclopédique, Que Sais-Je? (Universitaires de France, Paris, France).
Jung, K., R. Müller-Fiedler, P. Schlemmer, H. Ehrhardt, and H. Klar, 1985, J. Phys. B **18**, 2955.
Krasil'nikova, N. A., V. G. Levin, and N. A. Persiantseva, 1975, Zh. Eksp. Teor. Fiz. **69**, 1562 [Sov. Phys. JETP **42**, 796 (1976)].
Lahmam-Bennani, A., 1991, J. Phys. B **24**, 2401.
Lahmam-Bennani, A., L. Avaldi, E. Fainelli, and G. Stefani, 1988, J. Phys. B **21**, 2145.
Lahmam-Bennani, A., M. Cherid, and A. Duguet, 1987, J. Phys. B **20**, 2531.
Lahmam-Bennani, A., A. Duguet, and C. Dupré, 1992, J. Electron Spectrosc. Relat. Phenom. **58**, 17.
Lahmam-Bennani, A., H. F. Wellenstein, C. Dal Cappello, M. Rouault, and A. Duguet, 1983, J. Phys. B **16**, 2219.
Lahmam-Bennani, A., H. F. Wellenstein, A. Duguet, and M. Lecas, 1985, Rev. Sci. Instrum. **56**, 43.
Leung, K. T., 1991, in *Theoretical Models of Chemical Bonding,* Part 3, Molecular Spectroscopy, Electronic Structure, and Intramolecular Interactions, edited by Z. Maksic (Springer-Verlag, Berlin), p. 339.
Leung, K. T., and C. E. Brion, 1983, Chem. Phys. **82**, 87.
Lewis, G. N., 1916, J. Am. Chem. Soc. **38**, 762.
Lower, J., S. M. Bharathi, Yu Chen, K. J. Nygaard, and E. Weigold, 1991, Surf. Sci. **251/252**, 213.
Lower, J., and E. Weigold, 1989, J. Phys. E **22**, 421.
Madison, D. H., R. V. Calboun, and W. N. Shelton, 1977, Phys. Rev. A **16**, 552.
Martin, P., V. Veniard, A. Maquet, P. Francken, and C. J. Joachain, 1989, Phys. Rev. A **39**, 6178.
McCarthy, I. E., 1965, Rev. Mod. Phys. **37**, 388.
McCarthy, I. E., C. J. Noble, B. A. Phillips, and A. D. Turnbull, 1977, Phys. Rev. A **15**, 2173.
McCarthy, I. E., and M. J. Roberts, 1987, J. Phys. B, At. Mol. Opt. Phys. **20**, L251.
McCarthy, I. E., and E. Weigold, 1976, Phys. Rep. C **27**, 275.
McCarthy, I. E., and E. Weigold, 1989, *Electronic Structure of Materials Centre* (The Flinders University of South Australia), Report No. ESM-10.
McMillan, K., M. A. Coplan, J. H. Moore, and J. A. Tossell, 1990, J. Am. Chem. Soc. **94**, 8648.
McWeeny, R., 1949, Proc. Phys. Soc. London, Sect. A **62**, 519.
Minchinton, A., I. Fuss, and E. Weigold, 1982, J. Electron Spectrosc. Relat. Phenom. **27**, 1.
Moore, J. H., M. A. Coplan, T. L. Skillman, and E. D. Brooks, 1978, Rev. Sci. Instrum. **49**, 463.
Mota Furtado, F., and P. F. O'Mahony, 1989, J. Phys. B **22**, 3925.
Pan, C., and A. F. Starace, 1991, Phys. Rev. Lett. **67**, 185.
Persiantseva, N. M., N. A. Krasil'nikova, and V. G. Neudachin, 1979, Zh. Eksp. Teor. Fiz. **76**, 1047 [Sov. Phys. JETP **49**, 530 (1979)].
Peterkop, R., 1963, Izv. Akad. Nauk SSSR Ser. Fiz. **27**, 1012 [Bull. Acad. Sci. USSR, Phys. Ser. **27**, 987 (1963)].
Peterkop, R., 1971, J. Phys. B **4**, 513.
Pochat, A., R. J. Tweed, J. Peresse, C. J. Joachain, B. Pieaux, and F. W. Byron, Jr., 1987, J. Phys. B **16**, L775.
Popov, Yu. V., I. Bang, and J. J. Benayoun, 1981, J. Phys. B **14**, 4637.
Popov, Yu. V., and J. J. Benayoun, 1981, J. Phys. B **14**, 3513.
Popov, Yu. V., and V. F. Erokhin, 1983, Phys. Lett. A **97**, 280.
Rau, A. R. P., 1971, Phys. Rev. A **4**, 207.
Read, F. H., 1985, in *Electron Impact Ionization,* edited by G. Dunn and T. Märk (Springer, Berlin), p. 42.
Riou, M., 1965, Rev. Mod. Phys. **37**, 375.
Ritter, A. L., J. R. Dennison, and J. Dunn, 1984, Rev. Sci. Instrum. **55**, 1280.
Ritter, A. L., J. R. Dennison, and R. Jones, 1984, Phys. Rev. Lett. **53**, 2054.
Rösel, T., J. Röder, L. Frost, K. Jung, H. Ehrhardt, S. Jones, and D. H. Madison, 1992, Phys. Rev. A **46**, 2539.
Rudge, M. R. H., 1968, Rev. Mod. Phys. **40**, 564.
Ruhoff, H., and W. Nakel, 1987, J. Phys. B **20**, 2299.
Rutherford, E., 1911, Philos. Mag. **21**, 669.
Schröter, C. D., H. Graf, J. K. Bonfert, and W. Nakel, 1990, in *Second European Conference on (e,2e) Collisions and Related Problems,* edited by G. Stefani (Consiglio Nazionale delle Ricerche, Istituto di Metodologie Avanzate Inorganiche, Area della Ricerca di Roma), p. 65.
Schüle, E., and W. Nakel, 1982, J. Phys. B **12**, L639.
Selles, P., J. Mazeau, and A. Huetz, 1987, J. Phys. B **20**, 5183.
Shyn, T. W., and W. Sharp, 1991, Phys. Rev. A **43**, 2300.
Skillman, T. L., E. D. Brooks, M. A. Coplan, and J. H. Moore, 1978, Nucl. Instrum. Methods **155**, 267.
Smirnov, Yu. F., and V. G. Neudachin, 1966, Pis'ma Zh. Eksp. Teor. Fiz. **7**, 298 [JETP Lett. **3**, 192 (1966)].
Smith, A. D., M. A. Coplan, D. J. Chornay, J. H. Moore, J. A. Tossell, J. Mrozek, V. H. Smith, Jr., and N. S. Chant, 1986, J. Phys. B **19**, 969.

Stefani, G., and R. Camilloni, 1985, J. Phys. B **18**, 499.
Stefani, G., R. Camilloni, and A. Giardini-Guidoni, 1978, Phys. Lett. A **64**, 364.
Stefani, G., R. Camilloni, and Giardini-Guidoni, 1979, J. Phys. B **12**, 2583.
Thakkar, A. J., A. M. Simas, and V. H. Smith, 1981, Chem. Phys. **63**, 175.
Thirumalai, D., G. Staszewska, D. G. Truhlar, 1987, Comments At. Mol. Phys. **20**, 217.
Tossell, J. A., S. M. Lederman, J. H. Moore, M. A. Coplan, and D. J. Chornay, 1984, J. Am. Chem. Soc. **106**, 976.
Tossell, J. A., J. H. Moore, and M. A. Coplan, 1981, J. Electron Spectrosc. Relat. Phenom. **22**, 61.
van Wingerden, B., J. T. Kimman, M. van Tilburg, E. Weigold, C. J. Joachain, B. Piraux, and F. J. de Heer, 1979, J. Phys. B **12**, L627.
Völker, M., and W. Sandner, 1983, J. Phys. E **16**, 456.
Walters, J. R. J., A. Ast, C. T. Whelan, R. M. Dreizler, H. Graf, C. D. Schröter, J. Bonfert, and W. Nakel, 1992, Z. Phys. D **23**, 353.
Wannier, G. H., 1953, Phys. Rev. **90**, 873.
Weigold, E., 1984, Comments At. Mol. Phys. **15**, 223.
Weigold, E., 1990, J. Electron Spectrosc. Relat. Phenom. **51**, 629.
Weigold, E., S. Dey, A. J. Dixon, I. E. McCarthy, K. R. Lassley, and P. J. O. Teubner, 1976, Flinders University of South Australia, Institute for Atomic Studies Report FIAS-R-9, Abstract No. 266429, INIS Atomindex.
Weigold, E., S. T. Hood, P. J. Teubner, 1973, Phys. Rev. Lett. **30**, 475.
Weigold, E., C. J. Noble, S. T. Hood, and I. Fuss, 1979, J. Phys. B **12**, 291.
Weigold, E., K. Zhao, and W. von Niessen, 1991, J. Chem. Phys. **94**, 3469.
Weyrich, W., P. Pattison, and B. G. Williams, 1979, Chem. Phys. **41**, 271.
Zhang, X., C. T. Whelan, and H. R. J. Walters, 1990a, J. Phys. B **23**, L173.
Zhang, X., C. T. Whelan, and H. R. J. Walters, 1990b, J. Phys. B **23**, L509.
Zhang, X., C. T. Whelan, and H. R. J. Walters, 1992, Z. Phys. D **23**, 301.
Zheng, X., I. E. McCarthy, E. Weigold, and D. Zhang, 1990, Phys. Rev. Lett. **64**, 1358.